AD-A096 050 MASSACHUSETTS INST OF TECH LEXINGTON LINCOLN LAB F/G 15/3
DIGITAL SIMULATION MODELS OF CANDIDATE TACTICAL WEAPONS.(U)
SEP 80 R D'AMATO, J CAPON, C M SORRENTINO F19628-80-C-0002
UNCLASSIFIED TST-45 ESD-TR-80-170 NL

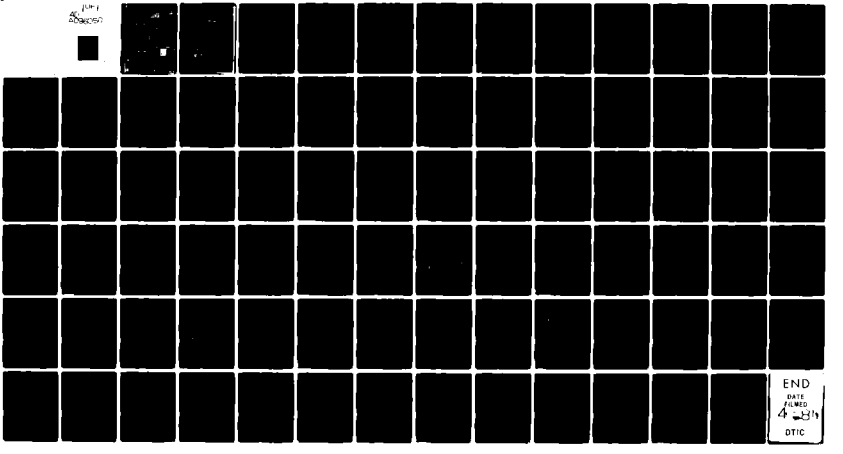

END
DATE FILMED
4-81
DTIC

LEVEL II

Project Report

TST-45

Sec 1473.

Digital Simulation Models of Candidate Tactical Weapons

R. D'Amato
J. Capon
C. M. Sorrentino

9 September 1980

Prepared for the Department of the Air Force
under Electronic Systems Division Contract F19628-80-C-0002 by

Lincoln Laboratory
MASSACHUSETTS INSTITUTE OF TECHNOLOGY
LEXINGTON, MASSACHUSETTS

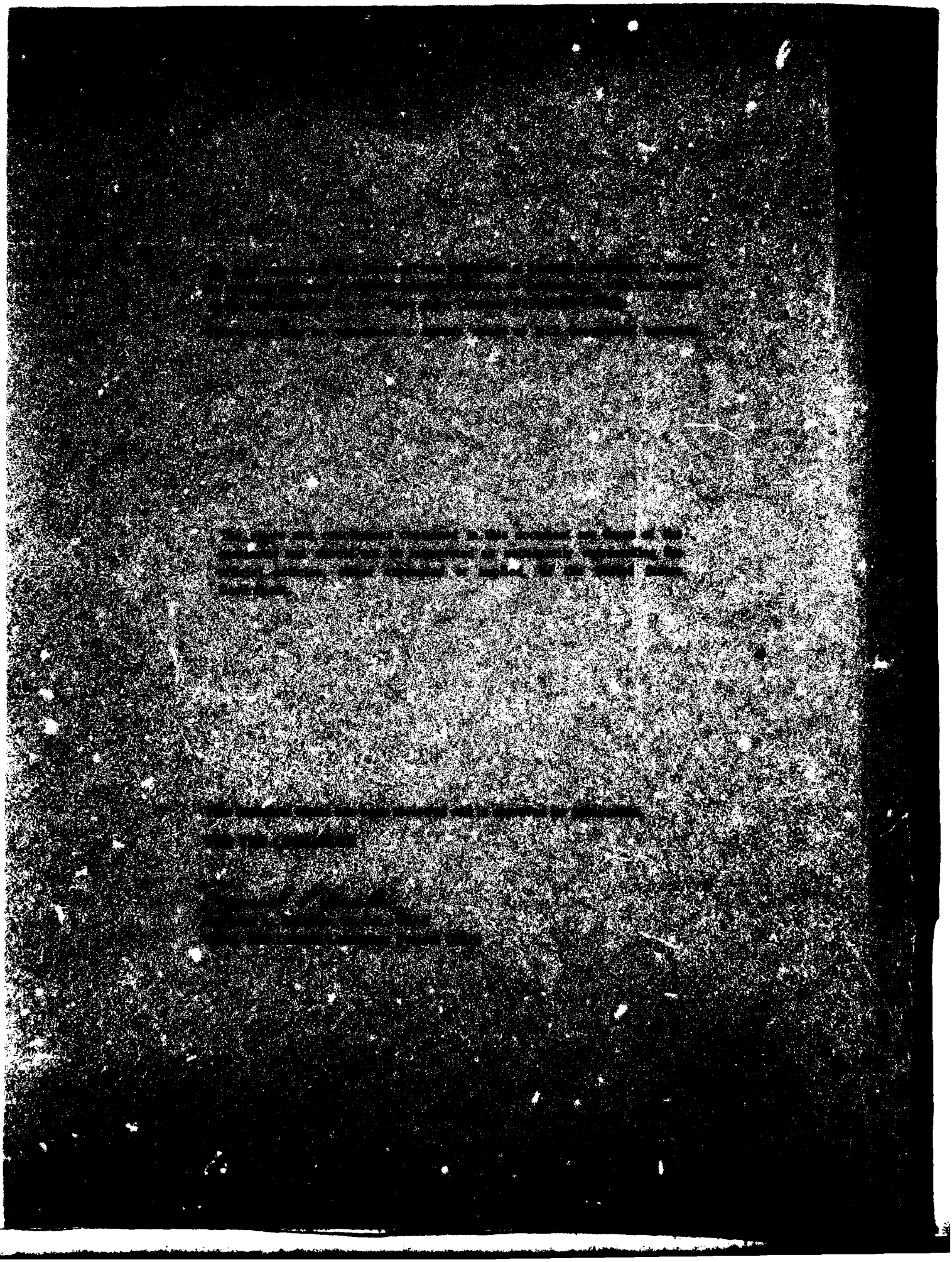

MASSACHUSETTS INSTITUTE OF TECHNOLOGY
LINCOLN LABORATORY

DIGITAL SIMULATION MODELS OF CANDIDATE TACTICAL WEAPONS

R. D'AMATO
Consultant

J. CAPON
C. M. SORRENTINO
(Group 44)

PROJECT REPORT TST-45
(Tactical Systems and Technology)

9 SEPTEMBER 1980

LEXINGTON MASSACHUSETTS

ABSTRACT

A five degree-of-freedom simulation has been constructed for each of four candidate tactical weapons for use in a program to develop/evaluate new techniques for emitter homing. The vehicle types include a powered missile, a projectile, a minidrone, and a glide bomb. The roll degree-of-freedom was eliminated from the simulation on the basis that each vehicle is stabilized in roll with low roll rates. The report provides detailed descriptions of the simulations including the aerodynamic and autopilot models, along with the numerical procedures used. Typical responses of the closed loop homing performance are given for each vehicle.

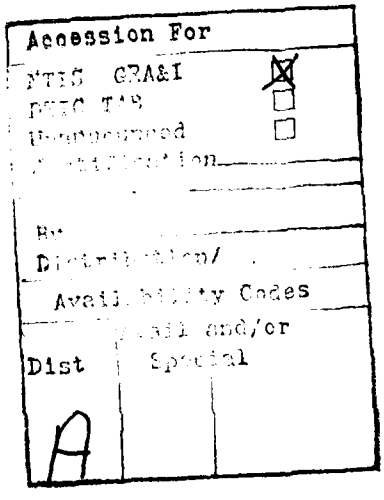

CONTENTS

LIST OF ILLUSTRATIONS

LIST OF ILLUSTRATIONS (cont'd)

LIST OF TABLES

1.0 INTRODUCTION

This report describes a five degree-of-freedom computer model of four different vehicle types. These models are intended for use in closed loop simulations to develop/evaluate new techniques for emitter homing [1,] and/or other autonomous seekers.

The four vehicles modeled are: 1) a powered missile, 2) a cannon-launched guided projectile, 3) a mini-drone, and 4) a glide bomb. The powered missile is based upon dynamic and aerodynamic characteristics that would be typical of the Maverick.[5] The projectile model is based on parameters associated with the Copperhead cannon-launched guided projectile [2, 6, 7, 8]. Preliminary data from the XBQM-106 was used to develop the mini-drone model [9]. Finally, the GBU-20 (GBU-15 PWW) [10, 11, 12] was the basis for the glide bomb. It is emphasized that while the simulations are considered realistic, they should not be considered as exact simulations for these specific vehicles.

In all of these models, the roll degree-of-freedom has been eliminated by assuming that the vehicle is roll stabilized with relatively low roll rates. In the case of the mini-drone, "side force" surfaces were incorporated to enhance the yaw maneuvering capability without the additional complexity of bank-to-turn maneuvers.

Section 2.0 provides a detailed description of the coordinate system, the equations of motion, the aerodynamic forces, the line-of-sight (LOS) sensor/processor and the guidance/autopilot model used for each vehicle type. Section 3.0 outlines the difference equations used for the simulations that were developed from the data in Section 2.0. Finally, Section 4.0 presents typical output from the simulation as mechanized.

2.0 MODEL DESCRIPTION

2.1 General

Figure 2.1 illustrates the overall geometry of the vehicle and its local, or body, coordinate system with respect to the fixed space coordinate system. Upper case letters (X, Y, Z) are used to denote the fixed coordinate system and lower case letters used for the body fixed coordinate system. Figure 2.2 is a companion figure used to further illustrate and define the geometrical parameters and their relationship to one another.

Since the vehicle is roll stabilized only two angles, the Euler angles θ and ψ, are needed to define the attitude of the vehicle body axes with respect to the space axis system. It is further noted that the body axes are rotated with respect to the fixed axes so that for θ and $\psi = 0$, the vehicle x-axis is -X, and the vehicle z-axis is -Z.

The Q and the R represent body, angular rotation rates (pitch and yaw) about the y and z axes, respectively. It is further noted that

$$\theta = \int Q dt \tag{2.1a}$$

$$\psi = \int \frac{R}{\cos\theta} dt \tag{2.1b}$$

The velocity of the vehicle center of mass (the origin of the body axis) is defined by the three velocity components u, v, w, along the x, y, z axes, respectively.

From Fig. 2.1, the velocity components, $\dot{X}_v$, $\dot{Y}_v$, $\dot{Z}_v$ of the vehicle center of mass are given by

$$\dot{X}_v = -u \cos\theta \cos\psi + v \sin\psi - w \sin\theta \cos\psi \tag{2.2a}$$

$$Y_v = u \cos\theta \sin\psi + v \cos\psi + w \sin\theta \sin\psi \tag{2.2b}$$

$$\dot{Z}_v = u \sin\theta - w \cos\theta \tag{2.2c}$$

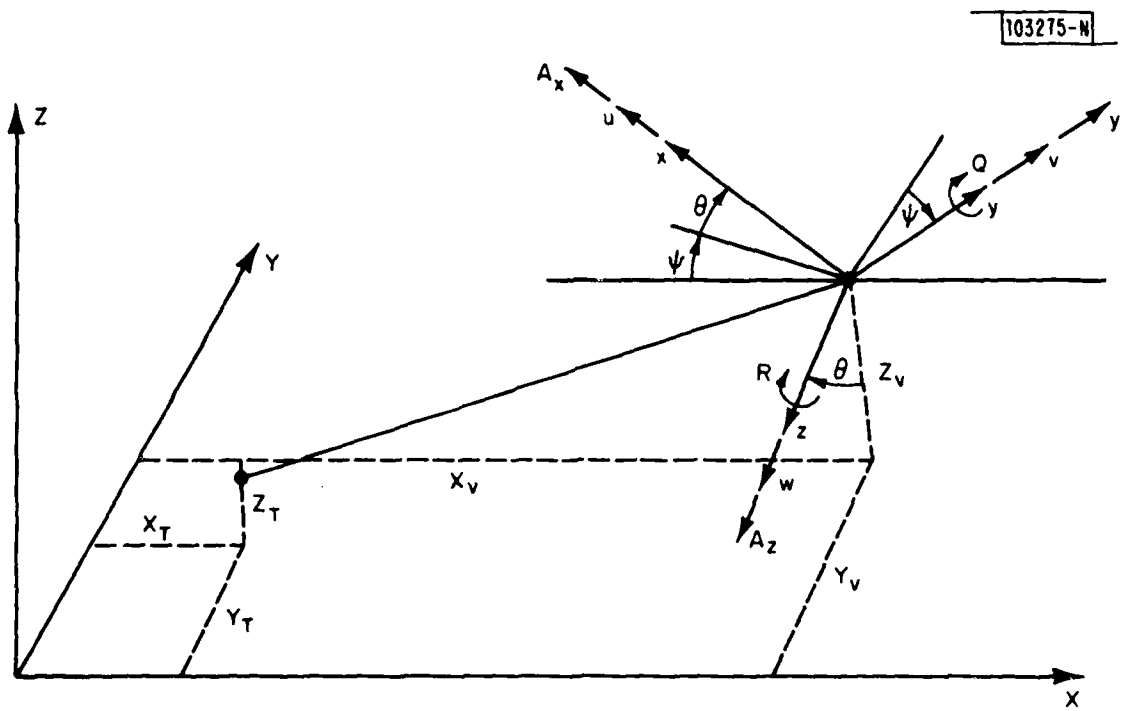

Fig. 2.1. Geometrical relationships.

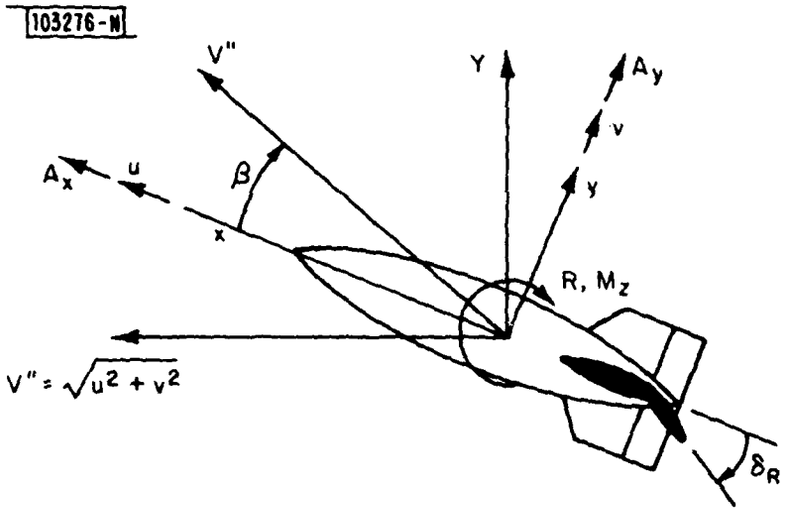

YAW PLANE

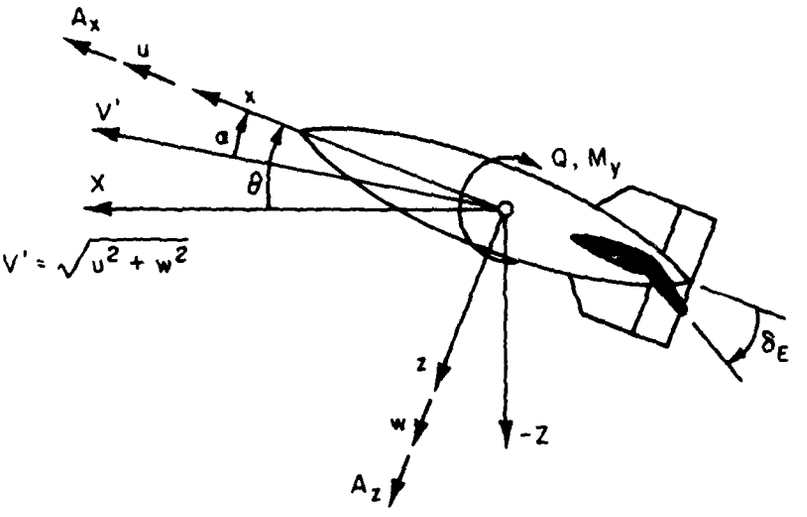

PITCH PLANE

Fig. 2.2. Vehicle body axes.

An overall block diagram of the simulation is shown in Fig. 2.3. As may be seen, there are four main blocks or models. The sensor feedback between the airframe and the autopilot/guidance blocks is shown in a general sense, that is, each model does not necessarily include all of the sensors as shown. The different models will utilize various combinations as will be seen below. The feedback paths without sensors are natural or inherent feedback due to the governing equations. For example, there is an altitude feedback path to the airframe model. Its function is to supply the information for the altitude dependent aerodynamic parameters. In the case of Q and R (pitch and yaw body angular rates) both the natural and the sensor feedback paths are used from the airframe to the LOS sensor/processor model. The reason for this is that the proportional navigation model used requires that the angle between the body axis and the LOS must be subtracted from the sensor measurement since a strapdown sensor has been assumed. This will be discussed further when the model details are considered.

The kinematic block of the simulation is given by equations 2.1 and 2.2 along with the following additional integration

$$X_v = \int \dot{X}_v \, dt$$

$$Y_v = \int \dot{Y}_v \, dt$$

$$Z_v = \int \dot{Z}_v \, dt$$

The blocks representing airframe and the guidance autopilot models will be considered in some detail in the following subsections. An elementary consideration of the LOS sensor/processor will be given here. A more detailed description is given in reference 2. The description given below will not discuss the details of how the measurement is made with the antenna sensor which interacts in a complex way with the target and terrain.

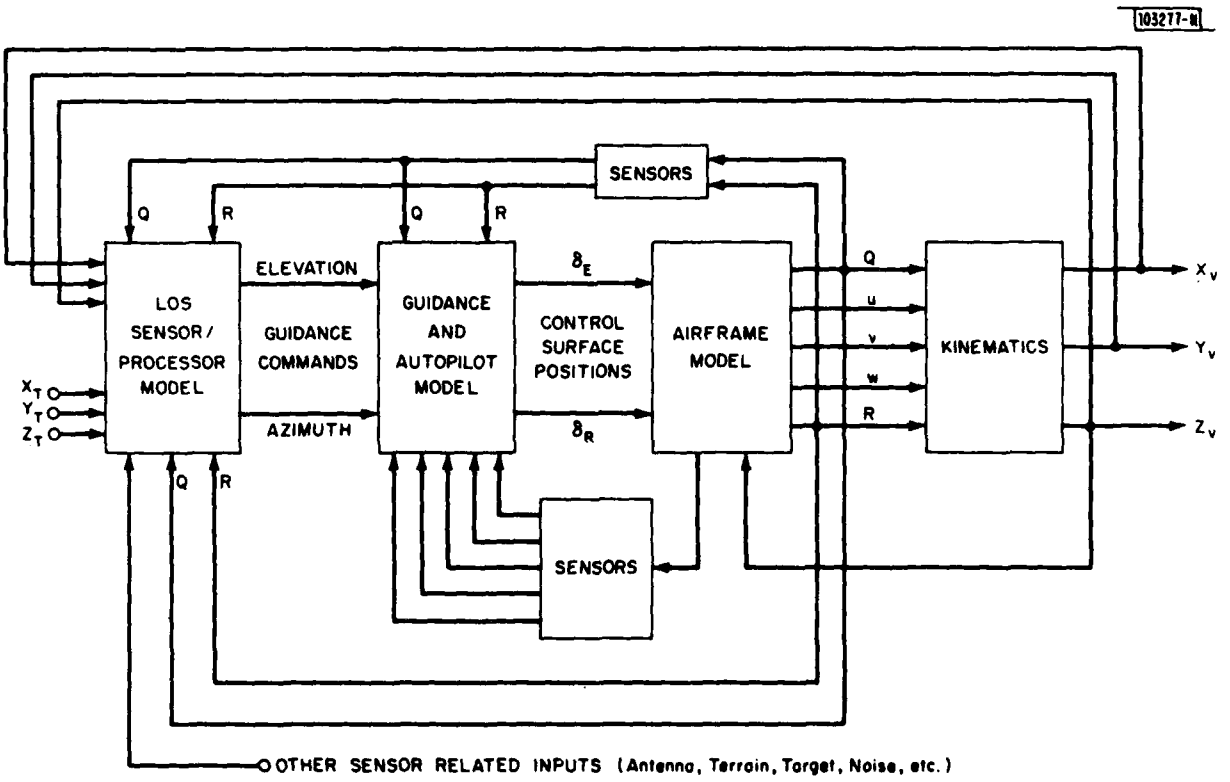

Fig. 2.3. Overall block diagram of simulation model.

2.2 Airframe Equations of Motion

The equations of motion of a rigid body with five degress of freedom (the roll degree of freedom is not included) are well known (Refs. 3, 4) and are as follows:

$$\dot{Q} = M_Y$$

$$\dot{R} = M_z$$

$$\dot{u} = A_x - g \sin\theta - \frac{1}{r_o} Qw + \frac{1}{r_o} Rv + T_x/m$$

$$\dot{v} = A_y - \frac{1}{r_o} Ru + T_y/m$$

$$\dot{w} = A_z + g \cos\theta + \frac{1}{r_o} Qu + T_z/m$$

where $r_o = 180/\pi$, the dot over the variable indicates differential with respect to time, and

Q = body pitch rate (in deg per sec)
R = body yaw rate (in deg per sec)
u = body axial velocity (along x direction - ft/sec)
v = body lateral velocity (along y direction - ft/sec)
w = body vertical velocity (along z direction - ft/sec)
M_y = normalized aerodynamic moment about Y axis or pitching moment
M_z = normalized yaw aerodynamic moment
A_x = normalized aerodynamic axial force
A_y = normalized aerodynamic sideforce (in yaw plane)
A_z = normalized aerodynamic normal force (in pitch plane)
T_y, T_y, T_z = x, y, z components of the thrust in lbs.

(NOTE: that if the thrust is misaligned with respect to the center of mass, additional moment contributions will be induced.) The normalized moments and forces are given as follows:

$$M_y = C_m \frac{q\,S\,\overline{c_y}\,r_o}{I_{yy}}$$

$$M_z = C_n \frac{q\,S\,\overline{c_z}\,r_o}{I_{zz}}$$

$$A_x = C_x \left(\frac{qS}{m}\right)$$

$$A_y = C_y \left(\frac{qS}{m}\right)$$

$$A_z = C_z \left(\frac{qS}{m}\right)$$

where $q = \frac{1}{2}\rho v^2$ = dynamic pressure (lbs/ft^2)

$v = \sqrt{u^2 + v^2 + w^2}$, total vehicle velocity (ft/sec)

ρ = air density at specified altitude (or z) (slugs per cubic foot)

S = reference area (ft^2)

m = vehicle mass = W/g (slugs)

w = vehicle weight (lbs)

g = gravity acceleration = 32.3 ft/sec^2

$\overline{c_y}$, $\overline{c_z}$ = reference lengths associated with the y and z directions, respectively (ft)

I_{yy}, I_{zz} = pitch and yaw moments of inertia, respectively (slug ft^2)

The C_m, C_n, C_x, C_y, C_z are aerodynamic coefficients which are functions, in general, of the angles of attack in pitch and yaw (α, β respectively) as well as Mach no (M) and the pitch and yaw control surface deflections (δ_E, δ_R), respectively. The Mach no. is defined as

$$M = V/a_o$$

where a_o is the speed of sound and is a function of altitude.

The values of the aerodynamic coefficients are usually determined by wind tunnel measurements, although analytical estimates are sometimes used. Depending upon the vehicle characteristics and velocity range, the coefficients, range from simple to complex requiring extensive two or three dimensional tables.

It is further to be noted that some of the inertial parameters can vary with time because of rocket motor burn off. For convenience, however, the pertinent values of the steady state parameters of all of the vehicles are given in Table 2.1.

2.3 Aerodynamic Forces

Up to this point, the formulation is general and applies to airframe model of all of the vehicles. The aerodynamic coefficients must be specialized for each of the vehicles which is done in appendices as follows:

Appendix 1	-	Missile
Appendix 2	-	Projectile
Appendix 3	-	Minidrone
Appendix 4	-	Glide Bomb

The data in these appendices provides the aerodynamic coefficients as functions of M, α, β, δ_E, δ_R. In addition, there are time varying inertial parameters for the Missile to account for the change of mass, moment inertia, and center of mass as the rocket motor burns. Note that this occurs in the first four seconds.

The variation of the speed of sound and air density is given by the following analytical expressions:

$$\rho = \rho_o (1 - 1.11 \bar{Z} + 0.36 \bar{Z}^2)$$

TABLE 2.1

GEOMETRIC AND INERTIAL PARAMETERS
(STEADY STATE VALUES)

PARAMETER	MISSILE	PROJECTILE	MINIDRONE	GLIDE BOMB
S (FT^2)	0.786	0.196	18.18	16.6
W (LBS)	398	135	135	3000
I_{YY} (SLUG FT^2)	53.5	6.13	25.5	646.2
I_{ZZ} (SLUG FT^2)	53.5	6.13	32.4	716.6
$\bar{C}_Y$	1	0.5	1.65	1.54
$\bar{C}_Z$	1	0.5	1.65	11.33

$$\rho_o = 0.002378$$

$$\bar{Z} = Z/40000$$

$$a_o = 1117 - (4.22 \times 10^{-3})Z \qquad 0 \leq Z \leq 36000$$

$$a_o = 965 \qquad 36000 \leq Z$$

where ρ is in slugs/ft^3 (= lb-sec^2/ft^4) and a_o is in ft/sec. Other formulas or tables could be used, but these provide a reasonable variation of the parameters needed for trajectory calculations.

2.4 LOS Sensor/Processor

As noted in Fig. 2.3, the inputs to the sensor/processor are the position in space of the vehicle and target, along with the actual and measured body rates in pitch and yaw. Basically, the task of the sensor/processor is to measure the line-of-sight between the vehicle and the target and from this measurement provide a command to the guidance computer. Since the sensor is fixed to the body, the body angle must be subtracted from the actual sensor measurement to obtain the LOS. This is done with the body rate sensors. Since the rate sensors, or gyros, are not perfect, the errors associated with them must be included in the simulation model. In addition, the sensor itself will introduce inaccuracies which also must be included. The actual simulation of the sensor measurement is extensive including reflections, multipath, terrain irregularities, and signal interference will not be considered here.

The true LOS in elevation and azimuth are given as

$$\lambda_z = -\text{TAN}^{-1} \frac{(Z_v - Z_T)}{\sqrt{(X_v - X_t)^2 + (Y_v - Y_T)^2}}$$

$$\lambda_y = \text{TAN}^{-1} \left(\frac{Y_v - Y_T}{X_v - X_T} \right)$$

where the subscripts indicate vehicle and target. To these LOS angles must be added the errors as noted above. The gyro errors in elevation and azimuth, θ_ε and ψ_ε, respecitvely, are

$$\theta_\varepsilon = \theta_{\varepsilon N} + \theta_{\varepsilon B} + \theta_{\varepsilon R}$$

$$\psi_\varepsilon = \psi_{\varepsilon N} + \psi_{\varepsilon B} + \psi_{\varepsilon R}$$

where the subscripts N, B, and R indicate noise, bias, and receiver, respectively. The noise and bias components from the rate gyro can be expressed as

$$\theta_{\varepsilon N} = \int Q_{\varepsilon N}\, dt$$

$$\theta_{\varepsilon B} = \int Q_{\varepsilon B}\, dt$$

$$\psi_{\varepsilon N} = \int \frac{R_{\varepsilon N}}{\cos\theta}\, dt$$

$$\psi_{\varepsilon B} = \int \frac{R_{\varepsilon B}}{\cos\theta}\, dt$$

where the $\cos\theta$ is needed to transform the body yaw angular rate to the azimuth plane. This bias value of pitch and yaw rate ($Q_{\varepsilon B}$, $R_{\varepsilon B}$) varies from sensor to sensor and from one period of time to another. The values are usually given as 1σ level or a maximum not to exceed level in degrees/sec or degrees/hr. The noise component of the error is, in general, correlated and can be expressed as [14]

$$\dot{Q}_{\varepsilon N} = -\frac{1}{\tau_G} Q_{\varepsilon N} + \sigma_G \sqrt{\frac{2}{\tau_G}}\, \eta$$

$$\dot{R}_{\varepsilon N} = -\frac{1}{\tau_G} R_{\varepsilon N} + \sigma_G \sqrt{\frac{2}{\tau_G}}\, \eta$$

where τ_G is the correlation time of the noise

σ_G is the rms level of the noise

η is unit intensity white noise

The spectrum for this model of the noise is

$$\phi(\omega) = \frac{2\ \tau_G\ \sigma_G^2}{1 + (\tau_G \omega)^2}$$

where ω is the circular frequency in radians per second. For simulation purposes, the unit intensity white noise level is generated from a random sequence (or random number) generator. This will be discussed further in Section 3.0.

Thus, the measured LOS can be expressed as

$$\lambda_{ZM} = \lambda_Z + \theta_{\epsilon N} + \theta_{\epsilon B} + \theta_{\epsilon R}$$

$$\lambda_{YM} = \lambda_Y + \psi_{\epsilon N} + \psi_{\epsilon B} + \psi_{\epsilon R}$$

The measured values are then filtered, differentiated and then filtered again. For example, the measured elevation LOS is processed as follows:

$$\text{Filter:}\quad \frac{d}{dt}\ (\lambda_{ZMF}) = -\frac{1}{\tau_f}\ (\lambda_{ZMF}) + \frac{1}{\tau_f}\ \lambda_{ZM}$$

$$\text{Differentiate Numerically:}\quad \dot{\lambda}_{ZMF} = \frac{\lambda_{ZMF_n} - \lambda_{ZMF_{n-1}}}{(t_n - t_{n-1})}$$

$$\text{Filter:}\quad \frac{d}{dt}\ (\dot{\lambda}_{ZMFF}) = -\frac{1}{\tau_f}\ (\dot{\lambda}_{ZMFF}) + \frac{1}{\tau_f}\ (\dot{\lambda}_{ZMF})$$

$$\text{Filter:}\quad \frac{d}{dt}\ (\dot{\lambda}_{ZMFFF}) = -\frac{1}{\tau_f}\ (\dot{\lambda}_{ZMFFF}) + \frac{1}{\tau_f}\ (\dot{\lambda}_{ZMFF})$$

The frequency at which this is done can be substantially slower than the general integration of the airframe equations of motion. The fact that several integrations of the system can occur over the sample time ($t_n - t_{n-1}$) is, in effect, a sample and hold. The value $\dot{\lambda}_{ZMFF}$ provides the proportional navigation signal to the guidance computer in pitch or elevation. The value $\dot{\lambda}_{ZMFFF}$ determines, in part, the switching to terminal guidance for the glide bomb.

The measured pitch "gimbal" angle is defined as

$$\theta_{GM} = \lambda_{ZM} - \theta$$

As for the line-of-sight, the measured sensor gimbal angle is filtered before being used as

$$\frac{d}{dt}(\theta_{GM1}) = -\frac{1}{\tau_A}\theta_{GM1} + \frac{1}{\tau_A}\theta_{GM}$$

$$\frac{d}{dt}(\theta_{GM2}) = -\frac{1}{\tau_B}\theta_{GM2} + \frac{1}{\tau_B}\theta_{GM1}$$

The filtered values of the gimbal angle are used for both mode switching and for trajectory shaping as indicated below.

2.5 Guidance/Autopilot

As for the aerodynamic forces, the guidance/autopilot model must be specialized for each vehicle type. The function of this model, as suggested by the subsection title, it twofold. The autopilot function is to insure that the vehicle is stable and controllable. Each of the four vehicle types considered requires some supplementary stability augmentation to insure adequate response over the complete flight regime. The guidance requirement is to convert the two commands from the LOS sensor/processor into appropriate positions of the control surfaces to guide the vehicle to the target. This part of the model is also used to represent any control surface dynamics and limits that are appropriate.

Figures 2.4, 2.5, 2.6, and 2.7 are models of the guidance/autopilot models for the missile, projectile, minidrone, and glide bomb, respectively. As may be seen, there is a fairly wide variation from model to model. Generally, the autopilots are more complex than the models given here. The simplifications are based primarily on eliminating the higher frequency components. For example, the rate gyros would probably have frequency components greater than 20 Hz. Thus, it, along with any shaping and filter currents, has been replaced by pure gains. The basic underlying assumption here is that adequate provision has been made to insure the stability of the autopilot. When this has been done properly, these higher frequency components are not needed for the guidance studies for which these models are designed. The parameters not given on the diagrams are given in Table 2.2. The mode switch sequences for the glide bomb are given in Table 2.3. The programmed yaw gain schedule given in Table 2.3 reduces the yaw gain during the activation of the pitch acceleration autopilot in the terminal phase of flight. The reason for this is to suppress the undesirable yaw/pitch coupling at high angles of attack.

As may be seen, the inputs for all of the models are the filtered line-of-sight rate in both pitch and yaw (azimuth and elevation) as well as the effective gimbal angle which is used to shape the trajectory. The output from the autopilot is the control surface deflections in pitch and yaw. The elevation and azimuth navigation gains, G_{ZN} and G_{YN}, have been made "noise adaptive" to suppress the deleterious effects of interference "noise" produced in a multiple emitter environment. This "noise" generally produces excessive maneuvers early in the trajectory before "locking on" to a specific target. These excessive maneuvers cause, in turn, a substantial reduction in velocity, and hence range, thereby decreasing the accuracy markedly. The approach here is to reduce the gain under these severe circumstances. The form of the gain is

$$G = \frac{G_o}{1 + \frac{V}{V_o}}$$

where $$V = \sum_{i=N-n_o}^{i=N} (\dot{\lambda} - \bar{\dot{\lambda}})^2$$

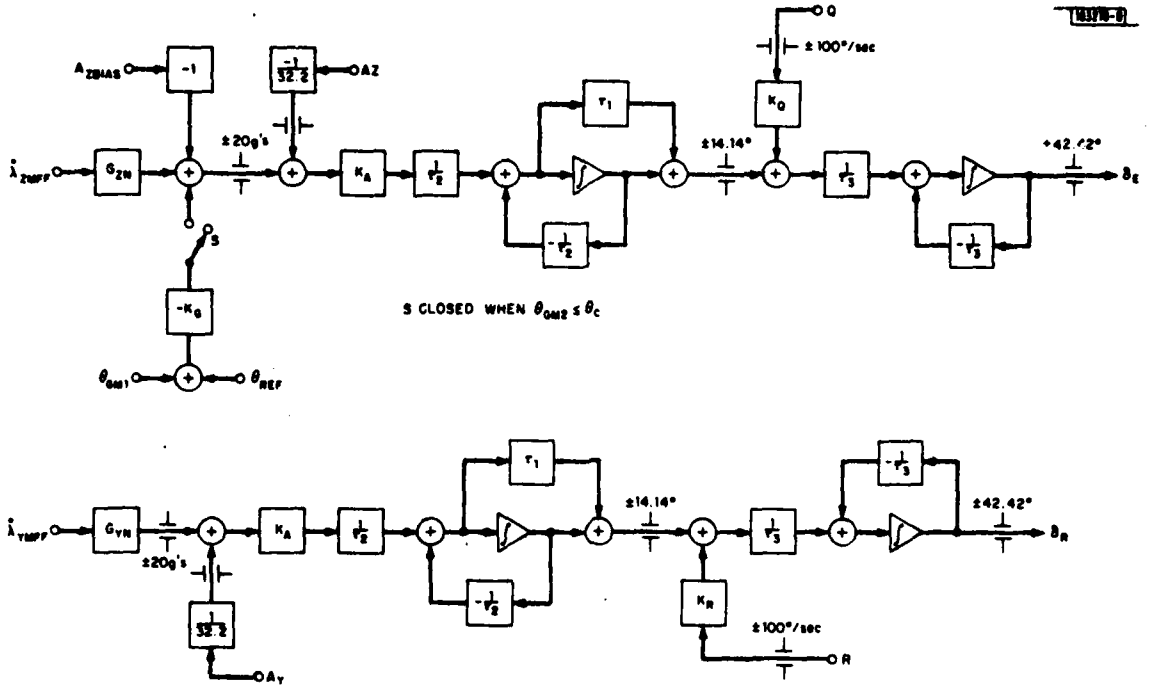

Fig. 2.4. Missile guidance/autopilot model.

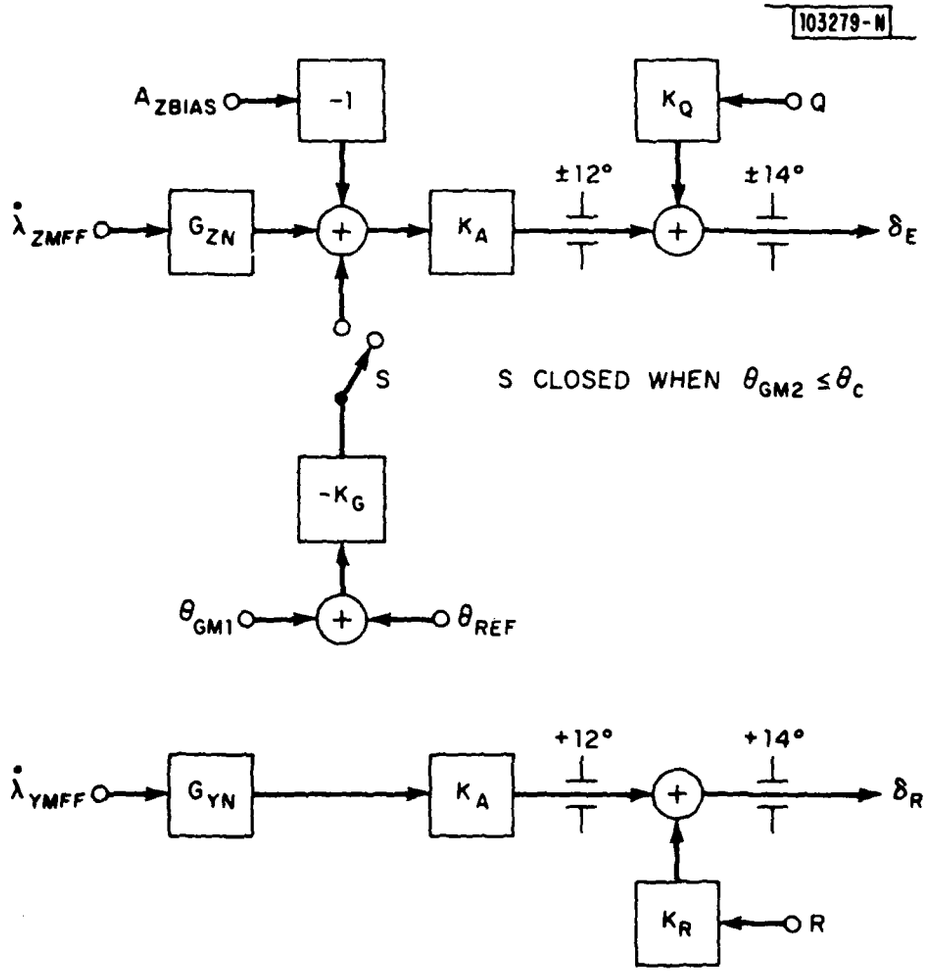

Fig. 2.5. Projectile guidance/autopilot model.

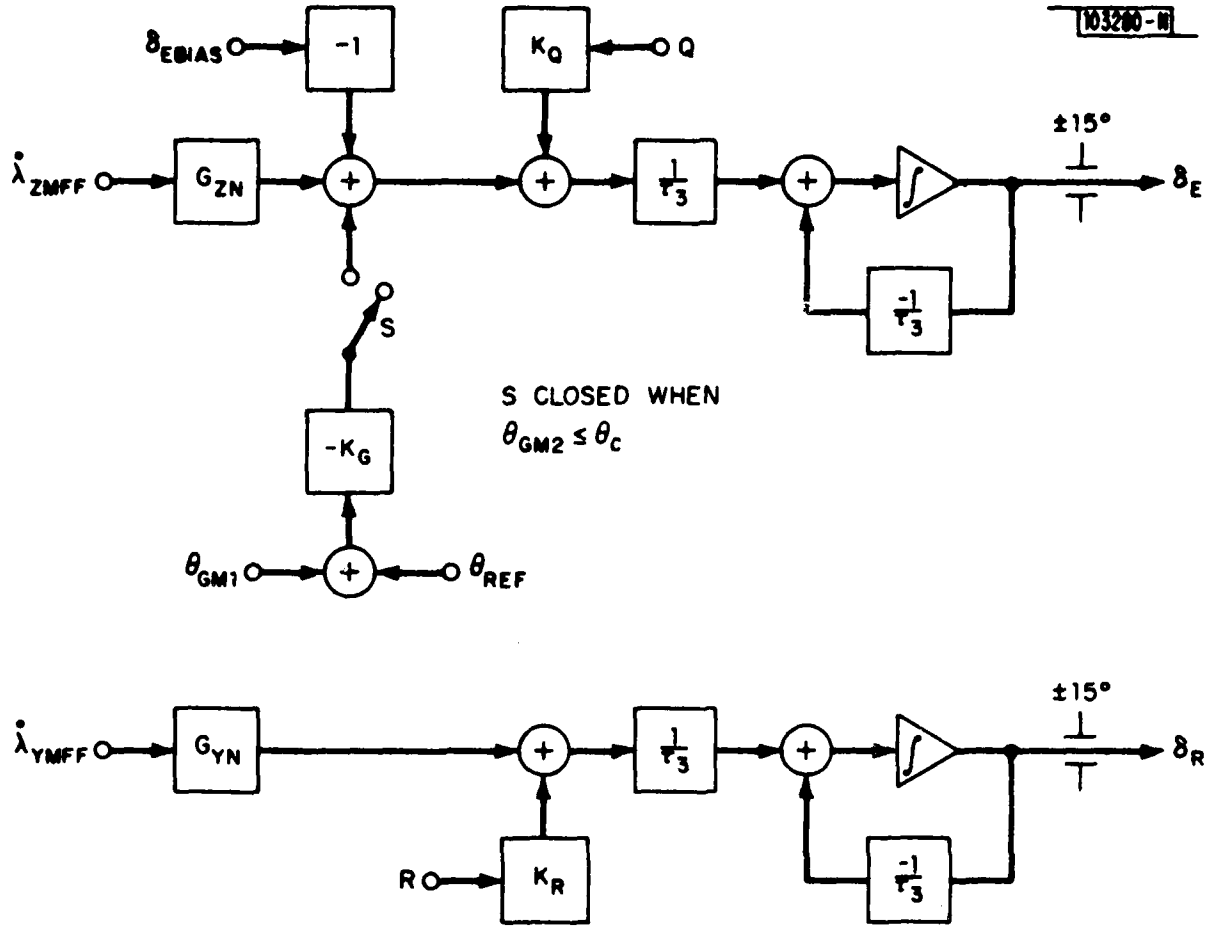

Fig. 2.6. Minidrone guidance/autopilot model.

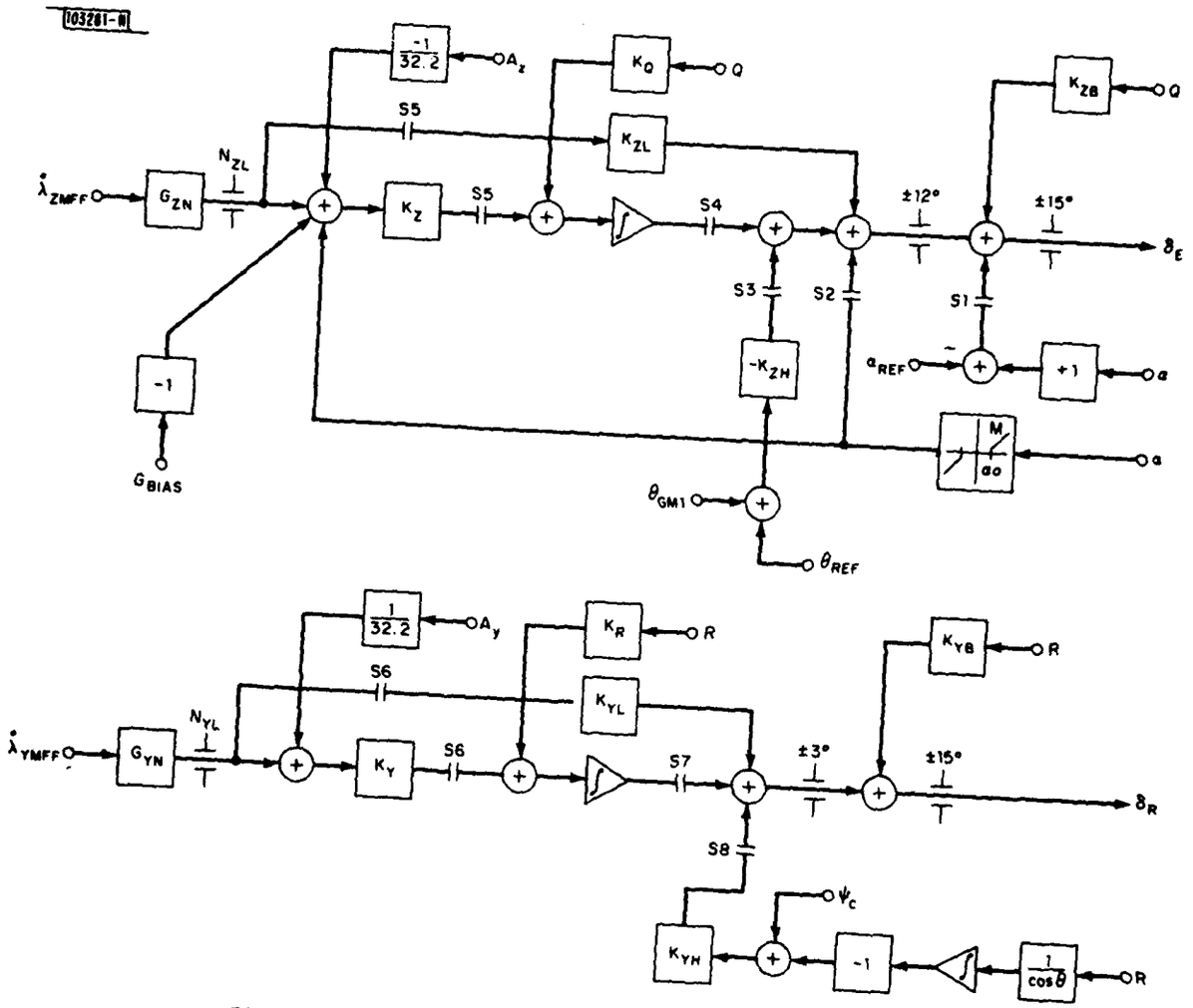

Fig. 2.7. Glide bomb guidance/autopilot model.

TABLE 2.2

VALUES FOR CONSTANTS USED IN SIMULATION

	UNITS	MISSILE	PROJECTILE	MINIDRONE	GLIDE BOMB
G_{OZ}	g/DEG/SEC	3.5	10.47	2 DEG/DEG/SEC	3
G_{OY}	g/DEG/SEC	3.5	9.13	2 DEG/DEG/SEC	2
K_A	DEG/g	2.2	0.8	---	---
K_Q	DEG/DEG/SEC	0.2	0.15	0.15	1
K_R	DEG/DEG/SEC	0.2	0.15	0.15	1
τ_1	SEC	0.03	---	---	---
τ_2	SEC	0.10	---	---	---
τ_3	SEC	0.05	---	0.1	---
K_G	g/DEG	0.0175	0.35	0	---
$1/\tau_f$	Hz	0.33/0.25*	0.33/0.25	0.25/0.17	0.33/0.25
$1/\tau_{A,B}$	Hz	0.33/0.50	0.33/0.5	0.25/0.25	0.33/0.50
K_{ZL}	DEG/g	---	---	---	1.25
K_{YL}	DEG/G	---	---	---	2.50
K_{ZB}	DEG/DEG/SEC	---	---	---	0.25
K_{YB}	DEG/DEG/SEC	---	---	---	0.25
K_Z	DEG/SEC/g	---	---	---	5
K_Y	DEG/SEC/g	---	---	---	5
K_{ZH}	DEG/SEC/DEG	---	---	---	1.0
K_{YH}	DEG/SEC/DEG	---	---	---	1.0
α_o	DEG	---	---	---	5.5/-12.0
M	---	---	---	---	2.00
α_{REF}	DEG	---	---	---	4
θ_{REF}	DEG	20	28.6	20	20
θ_c	DEG	-17.2	-11.50	**	-20
G_{BIAS}	g	3.5	4.25	---	1.0
N_{ZL}	g	---	---	---	2.5
N_{YL}	g	---	---	---	1.5

*PITCH/YAW

**Activated after 4 seconds of flight.

TABLE 2.3

MODE SWITCH SEQUENCE FOR GLIDE BOMB

	S1	S2	S3	S4	S5	S6	S7	S8
α HOLD	1	1	0	1	0	--	--	--
GIMBAL HOLD	0	1	1	0	0	--	--	--
ACCEL AUTOPILOT	0	1	0	1	1	--	--	--
Ψ COMMAND	--	--	--	--	--	0	0	1
ACCEL AUTOPILOT	--	--	--	--	--	1	1	0

Mode Sequencing

1. Flight initiated with α-Hold mode
2. Gimbal hold occurs when the following conditions are met

   2.1 $\theta_{GF2} \leq \theta_c$

   2.2 Flight time > 3 seconds

   2.3 $\theta < 9.7^0$

3. Acceleration auutopilot (terminal) occurs when the following conditions are met

   3.1 $\dot{\lambda}_{ZMFFF} < -0.344$ °/SEC

   3.2 Flight time > 3 seconds

   3.3 $\theta < -5.73^0$

   3.4 Gimbal hold must have been activated

4. ψ command not used for the trajectories considered
5. Yaw gain schedule

   5.1 $G_{YN} = 2.0$ $\quad 0 \leq t \leq t_{\text{gimbal hold}}$

   5.2 $G_{YN} = 0.75$ $\quad t_{\text{gimbal hold}} < t \leq t_{\text{terminal}} + 10$

   5.3 $G_{YN} = 1.75$ $\quad t_{\text{terminal}} < t$

N = current time interval

n_o = number of sample in the window

$\dot{\lambda}_i$ = ith value of the LOS rate

$\overline{\dot{\lambda}_i} = \frac{1}{n_o} \sum_{i=N-n_o}^{i=N} \dot{\lambda}_i$, or the average value of the LOS rate in the window

V_o = reference variance of the LOS rate

G_o = nominal noise free gain

For periods of very high noise levels, this law is quite effective in reducing the loss in energy caused by the noise induced maneuver drag.

It is to be noted that for some vehicles (notably the glide bomb and the projectile) that the use of the noise adjusted gain is not effective for the yaw channel and is, therefore, not used. The primary reason for this is that for sluggish vehicles (low maneuver capability), there is not sufficient excursion for target acquisition.

This variable gain can be implemented by means of recursion filters as

$$V_i = x_{2_i} - x_{1_i}^2$$

where V is the variance at the current instant, and

$$x_{2_i} = (1-A)\, x_{2_{i-1}} + A\dot{\lambda}_i^2$$

$$x_{1_i} = (1-A)\, x_{1_{i-1}} + A\dot{\lambda}_i$$

$$A = \exp(-T/\tau_V)$$

where τ_V is the filter time constant

T is the simulation interval

3.0 SIMULATION EQUATIONS AND PROCEDURE

The sequence of the simulation proceeds in the following steps:

1. Enter initial conditions
2. Update all variables
3. Guidance/autopilot commands
4. Aerodynamic forces
5. Equations of motion
6. Kinematics
7. LOS processor
8. Return to Step 2

Each one of these steps will be outlined and the required difference equations will be given.

3.1 Initial Conditions

The initial conditions for the simulation are as follows:

a. The position of the vehicle and target:

$$x_{V_o} \qquad x_{T_o}$$

$$Y_{V_o} \qquad Y_{T_o}$$

$$Z_{V_o} \qquad Z_{T_o}$$

b. The velocity, heading and angle-of-attack of the vehicle

$$V_o, \theta_o, \psi_o, \alpha_o, \beta_o$$

The velocity and angles-of-attack are used to determine the body velocity components as

$$u_o = V_o\sqrt{1 - \tan^2\alpha_o - \tan^2\beta_o}$$

$$v_o = u_o\tan\beta_o$$

$$w_o = u_o \tan\alpha_o$$

From these values the initial LOS and gimbal angles can be computed using the equations provided in Section 2.4.

c. The control surface positions

$$\delta_{Eo},\ \delta_{Ro}$$

d. All of the initial values of the filters are used in the simulation. Those values not specified are taken to be zero. In the case of the gyro noise which will be discussed further in Secion 3.6, the initial value of the noise filter $Q_{\epsilon N_o}$ and $R_{\epsilon N_o}$ are taken as σ_G, the rms of noise.

For the minidrone, a special procedure is followed. The drone is assumed to be flying at some load factor N_W, then the initial angle-of-attack and elevation angle are computed using the vehicle aerodynamic properties as follows:

Compute the dynamic pressure

$$q_o = \frac{1}{2}\rho V_o^2$$

using the initial velocity and the formulas given in Section 2.3. The initial angle-of-attack and control surface angle then found as

$$\alpha_o = \frac{\left(\frac{N_W W}{qS} - C_{L_o}\right) C_{m_{\delta_E}} + C_{m_o} C_{L_{\delta_E}}}{C_{L_\alpha} C_{m_{\delta_E}} - C_{m_\alpha} C_{L_{\delta_E}}}$$

$$\delta_{E_o} = \frac{C_{L_\alpha} C_{m_o} + C_{m_\alpha}\left(\frac{N_W W}{qS} - C_{L_o}\right)}{C_{L_{\delta_E}} C_{m_\alpha} - C_{M_{\delta_E}} C_{L_\alpha}}$$

3.2 Update all Variables

Updating of all variables consists in replacing the value of the variable in n+1 with the value of the variable in n, thus for a typical variable x

$$x_{n-1} = x_n$$

3.3 Guidance Equations

Using the block diagrams given in Section 2.5, the guidance equations were developed, and are given in Tables 3.1 to 3.4. In considering these tables, it is noted that the elevation and azimuth gains are adjusted in accordance with the procedure outlined in Section 2.5. The guidance commands ($\dot{\lambda}_{ZMFF}$, $\dot{\lambda}_{YMFF}$) are computed in the sensor/processor section of the simulation described in Section 3.7.

3.4 Aerodynamic Forces

The dynamic pressure and Mach no. are computed as:

$$\rho_n \quad \rho_o (1 - 1.111\ \bar{Z}_n + 0.36\ \bar{Z}_z^{\,2})$$

$$\rho_o = 0.002378$$

$$\bar{Z}_n = Z_{V_n}/40000$$

$$a_{o_n} = 1117 - (4.22 \times 10^{-3})\ Z_{V_n} \qquad 0 \leq Z_{V_n} \leq 36000$$

$$a_{o_n} = 965 \qquad 36000 \leq Z_{V_n}$$

$$M_n = V_n/a_{o_n}$$

$$q_n = \frac{1}{2} \rho_n V_n^{\,2}$$

Then with the most current values of α_n, β_n, δ_{E_n}, δ_{R_n}, M_n, the aerodynamic coefficients are computed or looked up in a table depending upon the form in which the coefficients are provided. The form for each of the vehicles is given in Appendices 1-4.

TABLE 3.1

MISSILE GUIDANCE EQUATIONS
(PITCH)

1. $A'_{ZC} = -G_{Z_n} \dot{\lambda}_{ZMFF_n} - A_{ZBIAS} - K_G (\theta_{GMI} + \theta_{REF})^*$

2. LIMIT A'_{ZC} to $\pm$ 20 g's = A'_{ZLC_n}

3. LIMIT $A_{Z_n}/32.2$ to $\pm$ 20 g's = A_{ZL_n}

4. $A_{ZC_n} = A'_{ZLC_n} - A_{ZL_n}$

5. $x_n = F_2 x_n + (1 - F_2) K_A A_{ZC_n}$

6. $\delta'_{E_n} = (1 - \frac{\tau_1}{\tau_2}) x_n + \frac{\tau_1}{\tau_2} K_A A_{ZC_n}$

7. LIMIT δ'_{E_n} to $\pm$ 14.14° = δ'_{EL_n}

8. LIMIT Q_n to 100°/SEC = Q_{L_n}

9. $\delta_{E_n} = F_3 \delta_{E_{n-1}} + (1 - F_3) (\delta'_{EL_n} + K_Q Q_{L_n})$

10. LIMIT δ_{E_n} to $\pm$ 42.42° = δ_{EL_n}

$$F_2 = e^{-T/\tau_2} \qquad F_3 = e^{-T/\tau_3}$$

*Note that this term included only after

$\theta_{GM2} < \theta_c$

TABLE 3.1 (cont'd)

MISSILE GUIDANCE EQUATIONS
(YAW)

1. $A'_{YC} = -G_{Y_n} \dot{\lambda}_{YMFF}$

2. LIMIT A'_{YC} to $\pm$ 20 g's = A'_{YCL_n}

3. LIMIT $A_{Y_n}/32.3$ to $\pm$ 20 g's = A_{YL_n}

4. $A_{YC_n} = A'_{YCL_n} + A_{YL_n}$

5. $x_n = F_2 x_n + (1 - F_2) K_A A_{YC_n}$

6. $\delta'_{R_n} = (1 - \frac{\tau_1}{\tau_2}) x_n + \frac{\tau_1}{\tau_2} K_A A_{YC_n}$

7. LIMIT δ'_{R_n} to $\pm$ 14.14" = δ'_{RL_n}

8. LIMIT R_n to 100°/SEC = R_{L_n}

9. $\delta_{R_n} = F_3 \delta_{R_{n-1}} + (1 - F_3)(\delta'_{RL_n} + K_R R_{L_n})$

10. LIMIT δ_{R_n} to $\pm$ 42.42° = δ_{RL_n}

$$F_2 = e^{-T/\tau_2} \qquad F_3 = e^{-T/\tau_3}$$

TABLE 3.2

PROJECTILE GUIDANCE EQUATIONS

A. PITCH

1. $A_{ZC_n} = -G_{Z_n} \dot{\lambda}_{ZMFF} - A_{ZBIAS} - K_G (\theta_{GM1} + \theta_{REF})^*$

2. $\delta'_{E_n} = K_A A_{ZC_n}$

3. LIMIT δ'_{E_n} to $\pm$ 12° = δ'_{EL_n}

4. $\delta_{E_n} = \delta'_{EL_n} + K_Q Q_n$

5. LIMIT δ_{E_n} to $\pm$ 14° = δ_{EL_n}

B. YAW

1. $A_{YC_n} = -G_{Y_n} \dot{\lambda}_{YMFF}$

2. $\delta'_{R_n} = K_A A_{YC_n}$

3. LIMIT δ'_{R_n} to $\pm$ 12° = δ'_{RL_n}

4. $\delta_{R_n} = \delta'_{RL_n} + K_R R_n$

5. LIMIT δ_{R_n} to $\pm$ 14° = δ_{RL_n}

*Note that this term is included only when

$$\theta_{GM2} < \theta_c$$

TABLE 3.3

MINIDRONE GUIDANCE EQUATIONS

A. PITCH

1. $\delta_{EC_n} = -G_{ZN} \dot{\lambda}_{ZMFF} - \delta_{EBIAS} - K_G (\theta_{GM1} + \theta_{REF})^* + K_Q Q_n$

2. $\delta_{E_n} = F_3 \delta_{E_{n-1}} + (1 - F_3) \delta_{EC_n}$

3. LIMIT δ_{E_n} to $\pm$ 15° = δ_{EL_n}

B. YAW

1. $\delta_{RC_n} = -G_{Y_n} \dot{\lambda}_{YMFF} + K_R R_n$

2. $\delta_{R_n} = F_3 \delta_{R_{n-1}} + (1 - F_3) \delta_{RC_n}$

3. LIMIT δ_{R_n} to $\pm$ 15° = δ_{RL_n}

$$F_3 = e^{-T/\tau_3}$$

*Note that this term is included only when $\theta_{GM2} < \theta_c$

TABLE 3.4

GLIDE BOMB GUIDANCE EQUATIONS*
(PITCH)

A. ANGLE-OF-ATTACK HOLD (α-HOLD S1, S2, S4=1)

1. CHECK α

IF $\alpha_n \leq \alpha_{L1}$ $\quad x_n = M_o(\alpha_n - \alpha_{L1})$

IF $\alpha_n \geq L2$ $\quad x_n = M_o(\alpha_n - \alpha_{L2})$

OTHERWISE $x_n = 0$

2. $\delta''_{E_n} = \delta''_{E_{n-1}} + \frac{T}{2} K_Q (Q_n + Q_{n-1})$

3. $\delta'_{E_n} = \delta''_{E_n} + x_n$

4. LIMIT δ'_{E_n} to $\pm$ 12° = δ'_{EL_n}

5. $\delta_{E_n} = \delta'_{EL_n} + K_{ZB} Q_n - \alpha_{REF} + \alpha_n$

6. LIMIT δ_{E_n} to $\pm$ 15° = δ_{EL_n}

B. GIMBAL HOLD (S2, S3=1)

1. CHECK α

IF $\alpha_n \leq \alpha_{L1}$ $\quad x_n = M_o(\alpha_n - \alpha_{L1})$

IF $\alpha_n \geq \alpha_{L2}$ $\quad x_n = M_o(\alpha_n - \alpha_{L2})$

OTHERWISE $x_n = 0$

2. $\delta'_{E_n} = x_n - K_{ZH} (\theta_{GM1} + \theta_{REF})$

3. LIMIT δ'_{E_n} to $\pm$ 12° = δ_{EL_n}

*See mode sequencing given in Table 2.3

TABLE 3.4 (cont'd)

GLIDE BOMB GUIDANCE EQUATIONS
(YAW)

A. ψ COMMAND (S7, S8=1)

1. $\delta''_{R_n} = K_{YH} (\psi_c - \psi_n)$

2. LIMIT δ''_{R_n} to $\pm$ 3° = δ'_{RL_n}

3. $\delta_{R_n} = \delta'_{RL_n} + K_{YB} = R_n$

4. LIMIT δ_{R_n} to $\pm$ 15° = δ_{RL_n}

B. ACCELERATION AUTOPILOT (S6, S7=1)

1. $A_{YC_n} = G_{Y_n} \dot{\lambda}_{YMFF}$

2. LIMIT A_{YC_n} to $N_{YL} = A_{YCL_n}$

3. $\delta'''_{R_n} = K_Y (A_{YCL_n} - A_{Z_n}/32.2) + K_r R_n$

4. $\delta''_{R_n} = \delta''_{R_{n-1}} + \frac{T}{2} (\delta'''_{R_n} + \delta'''_{R_{n-1}})$

5. $\delta'_{R_n} = \delta''_{R_n} + K_{YL} A_{YCL_n}$

6. LIMIT δ'_{R_n} to $\pm$ 3° = δ'_{RL_n}

7. $\delta_{R_n} = \delta'_{RL_n} + K_{YB} R_n$

8. LIMIT δ_{R_n} to $\pm$ 15° = R_{RL_n}

TABLE 3.4 (cont'd)

GLIDE BOMB GUIDANCE EQUATIONS
(YAW)

4. $\delta_{E_n} = \delta'_{E_n} + K_{ZB}\, Q_n$

5. LIMIT δ_{E_n} to $\pm$ 15° = δ_{EL_n}

c. ACCELERATION AUTOPILOT (S2, S4, S5-1)

1. CHECK α

IF $\alpha_n \leq \alpha_{L1}$ $x_n = M_o(\alpha_n - \alpha_{L1})$

IF $\alpha_n \geq \alpha_{L2}$ $x_n = M_o(\alpha_n - \alpha_{L2})$

OTHERWISE $x_n = 0$

2. $A_{ZC_n} = -G_{Z_n} \mathring{\lambda}_{ZMFF}$

3. LIMIT A_{ZC_n} to $N_{ZL} = A_{ZCL_n}$

4. $A'_{ZC_n} = K_Z\,(A_{ZCL_n} - A_{Z_n}/32.3 - A_{ZBIAS} + x_n) + K_Q\, Q_n$

5. $\delta''_{E_n} = \delta''_{E_{n-1}} + \frac{T}{2}\,(A'_{ZC_n} + A_{ZC_{n-1}})$

6. $\delta'_{E_n} = \delta''_{E_n} + x_n + K_{ZL}\, A_{ZCL_n}$

7. LIMIT δ'_{E_n} to $\pm$ 12° = δ'_{EL_n}

8. $\delta_{E_n} = \delta'_{EL_n} + K_{ZB}\, Q_n$

9. LIMIT δ_{E_n} to $\pm$ 15° = δ_{EL_n}

When the coefficients have been obtained, the aerodynamic forces and moments are computed as follows:

$$M_{Y_n} = C_{m_n} \frac{q_n S \bar{C}_Y r_o}{I_{YY}}$$

$$M_{Z_n} = C_{n_n} \frac{q_n S \bar{C}_z^n r_o}{I_{ZZ_n}}$$

$$A_{x_n} = C_{Y_n} \frac{q_n S}{m_n}$$

$$A_{Y_n} = C_{Y_n} \frac{q_n S}{m_n}$$

$$A_{Z_n} = C_{Z_n} \frac{q_n S}{m_n}$$

where the subscript has been included on I_{YY}, I_{ZZ} to account for the variation in the inertial parameters caused during the burn period of powered vehicles.

3.5 Equations of Motion

The angular and translational accelerations $\dot{Q}_n$, $\dot{R}_n$, $\dot{u}_n$, $\dot{v}_n$, $\dot{w}_n$ are computed from the equations given in Section 2.2 using the most current values of the variables. These equations are then integrated as

$$Q_n = Q_{n-1} + \frac{T}{2}(\dot{Q}_n + \dot{Q}_{n-1})$$

$$\theta_n = \theta_{n-1} + \frac{T}{2}(Q_n + Q_{n-1})$$

$$R_n = R_{n-1} + \frac{T}{2}(\dot{R}_n + \dot{R}_{n-1})$$

$$\psi_n = \psi_{n-1} + \frac{T}{2}\left(\frac{R_n}{\cos\theta_n} + \frac{R_{n-1}}{\cos\theta_{n-1}}\right)$$

$$u_n = u_{n-1} + \frac{T}{2}(\dot{u}_n + \dot{u}_{n-1})$$

$$v_n = v_{n-1} + \frac{T}{2}(\dot{v}_n + \dot{v}_{n-1})$$

$$w_n = w_{n-1} + \frac{T}{2}(\dot{w}_n + \dot{w}_{n-1})$$

3.6 Kinematics

Having the velocity components in body axes (u_n, v_n, w_n,) as well as the orientation of the body axis (θ_n, Ψ_n); the velocity of the vehicle in space $\dot{X}_{v_n}$, $\dot{Y}_{v_n}$, $\dot{Z}_{v_n}$, can be computed from the transformation equations given in Section 2.1. Finally the position of the vehicle in space is obtained by integration as

$$X_{v_n} = X_{v_{m-1}} + \frac{T}{2}(\dot{X}_{v_n} + \dot{X}_{v_{n-1}})$$

and the same for the Y_{v_n} and Z_{v_n} components.

3.7 LOS Processor

As noted in Section 2.4, the measured LOS angles are given by

$$\lambda_{ZM_n} = \lambda_{Z_n} + \theta_{\varepsilon N_n} + \theta_{\varepsilon B} + \theta_{\varepsilon R}$$

$$\lambda_{YM_n} = \lambda_{Y_n} + \theta_{\varepsilon N_n} + \theta_{\varepsilon B} + \psi_{\varepsilon R}$$

where λ_{Z_n} and λ_{Y_n} are computed from the equations given in Section 2.4.

The differential equations for the noise components of the body rate measurements must be cast into a difference form for use in the digital simulation. The white noise input into these equations is approximated by the sequence from a random number generator as

$$\eta_n = K(R_n - 0.5)$$

where R_n is a random number between 0 and 1 and K is a constant chosen to make the spectral density of the sequence unity. For a sample time of T, the spec-

trum of the sequence η_n is a flat double-sided function between $\pm \omega_o$ (the folding frequency given as $(2\pi/T)/2$rad/sec). The intensity of the noise is then

$$S_o = \frac{K^2}{24\omega_o} \qquad -\frac{\pi}{T} < \omega_o < \frac{\pi}{T}$$

For unit intensity ($S_o = 1$)

$$K = \sqrt{\frac{24\pi}{T}}$$

Then, in difference form

$$Q_{\varepsilon N_n} = A\, Q_{\varepsilon N_{n-1}} + (1-A)\, \sigma_G\, 2\tau_G\, \eta_n$$

$$R_{\varepsilon N_n} = A\, R_{\varepsilon N_{n-1}} + (1-A)\, \sigma_G\, 2\theta_G\, \eta_n'$$

where $A = e^{-T/\tau_G}$ and η_n' distinguishes the sequence of η_n' from η_n. The initial condition of these filters is $Q_{\varepsilon N_o} = R_{\varepsilon N_o} = \sigma_G$. Then,

$$\theta_{\varepsilon N_n} = \theta_{\varepsilon n_{n-1}} + \frac{T}{2}\,(Q_{\varepsilon N_o} + Q_{\varepsilon N_{n-1}})$$

$$\psi_{\varepsilon B_n} = \psi_{\beta N_{n-1}} + \frac{T}{2}\,(R_{\varepsilon N_n}/\cos\theta_n + R_{\varepsilon N_{n-1}}/\cos\theta_{n-1})$$

For the gyro bias component

$$\theta_{\varepsilon B_n} = \theta_{\varepsilon B_{n-1}} + TQ_{\varepsilon B_o}$$

$$\psi_{\varepsilon B_n} = \psi_{\varepsilon B_{n-1}} + \frac{T}{2}\,(R_{\varepsilon B_o}/\cos\theta_n + R_{\varepsilon B_o}/\cos\theta_{n-1})$$

where $Q_{\varepsilon B_o}$ and $R_{\varepsilon B_o}$ are the gyro rate biases assumed for the particular simulation run. Finally, for wide band receiver noise

$$\theta_{\epsilon R_n} = \sqrt{12}\ \sigma_R\ (R_n - 0.5)$$

$$\psi_{\epsilon R_n} = \sqrt{12}\ \sigma_R\ (R'_n - 0.5)$$

and σ_R is the rms value of the receiver noise and, again, the R'_n distinguishes the random sequence for $\psi_{\epsilon R_n}$ from that of $\theta_{\epsilon R_n}$.

The next step is to filter, differentiate and filter as noted in Section 2.4 the difference equations for elevation

$$\lambda_{ZMF_n} = A_Z\ \lambda_{ZMF_{n-1}} + (1-A_Z)\ (\lambda_{ZM_n})$$

$$\dot{\lambda}_{ZMF_n} = (\lambda_{ZMF_n} - \lambda_{ZMF_{n-1}})/\Delta t$$

$$\dot{\lambda}_{ZMFF_n} = A_Z\ \dot{\lambda}_{ZMFF_{n-1}} + (1-A_Z)\ (\dot{\lambda}_{ZMF_n})$$

$$\dot{\lambda}_{ZMFFF_n} = A_Z\ \dot{\lambda}_{ZMFFF_{n-1}} + (1-A_Z)\ \dot{\lambda}_{ZMFF_n}$$

where $A_z = e^{-\Delta t/\tau_f}$ and $\Delta t = t_n - t_{n-1}$. Similar equations are used for azimuth. The values of the LOS rates in elevation and azimuth are used to povide commands to the guidance computer.

In a like manner, the filtered gimbal angles are computed as

$$\theta_{GM1_n} = A_A\ \theta_{GM1_{n-1}} + (1-A_A)\ (\lambda_{ZM_n} - \theta_n)$$

$$\theta_{GM2_n} = A_B\ \theta_{GM2_{n-1}} + (1-A_B)\ \theta_{GM1_n}$$

where $A_A = e^{-\Delta t/\tau_A}$ and $A_B = e^{-\Delta t/\tau_B}$

4.0 SAMPLE NUMERICAL RESULTS

Figures 4.1 to 4.4 present sample simulation output for the four vehicle types described in the previous sections. These runs include only the effects of gyro noise and bias. Except for the projectile for which the gyro bias was taken as 0.1°/sec, the bias value was 0.06°/sec and the noise rms was 10°/hr with a correlation time of 15 minutes [12]. Only the bias contributes significantly to the error.

As may be seen, Fig. 4.1(a) shows the overall trajectory in the pitch of elevation plane. The gyro bias caused the vehicle to climb shortly after launch. The numbers printed on the trajectory indicate flight time after launch in seconds (or for very long flights in the case of the minidrone in Fig. 4.3(a), in minutes).

The projectile trajectory in Fig. 4.2(a) has its starting condition at a height and speed consistent with roughly the midpoint of its flight [9]. Since the minidrone is a loiter vehicle, its starting condition was approximately level (1 g) flight.

The starting points of the missile and glide bomb trajectories (4.1(a) and 4.4(a), respectively) were based upon typical conditions at the end of midcourse.

Figures 4.1(b), 4.2(b), 4.3(b), and 4.4(b) give the time history of the vehicle velocity, the elevation acceleration command and the pitch load factor actually achieved by the vehicle. In the case of the missile (fig. 4.1(b)), the velocity is shown increasing from about 800 ft/sec at the start to a maximum of about 1360 ft/sec after 4 seconds, which results from the rocket propulsion after launch. After burn out, the velocity markedly decreases with time until a fairly stable level of 574 ft/sec is achieved. The initial value of the commanded load factor represents the bias command used to shape the trajectory. The dip in the pitch load factor during the time after burn out is due to the correcting command needed to bring the vehicle back on course from the climbing maneuver caused by the gyro bias error.

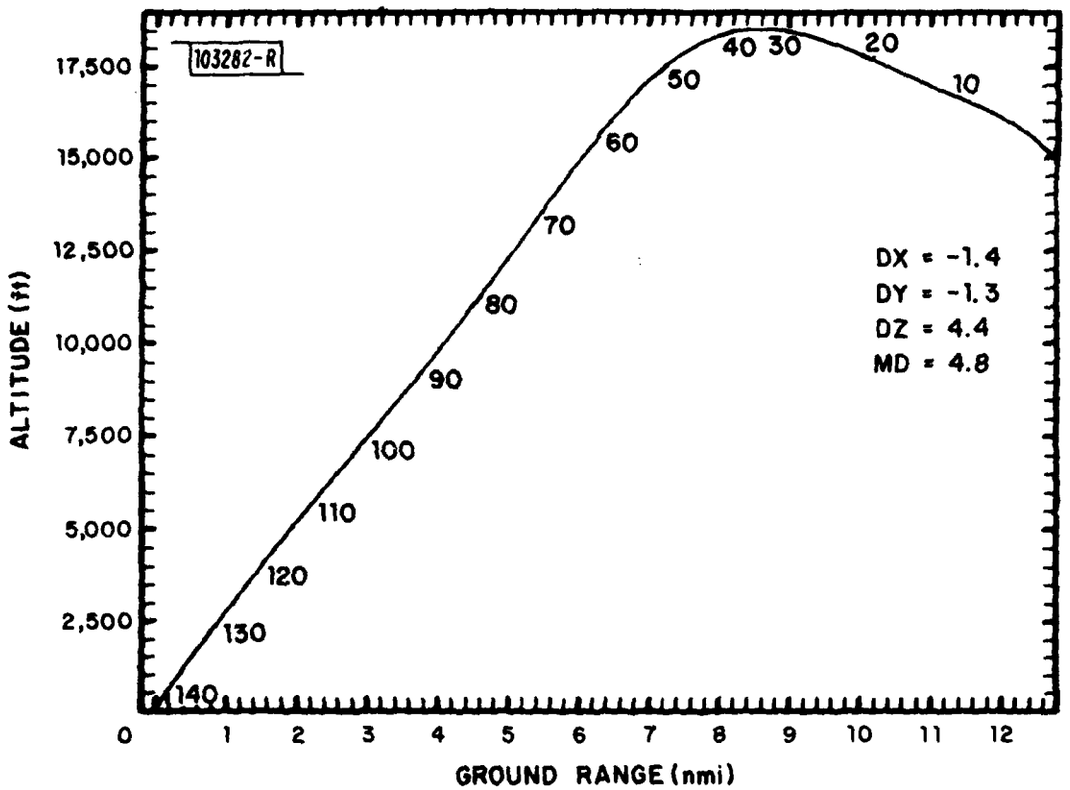

Fig. 4.1(a). Sample output for missile.

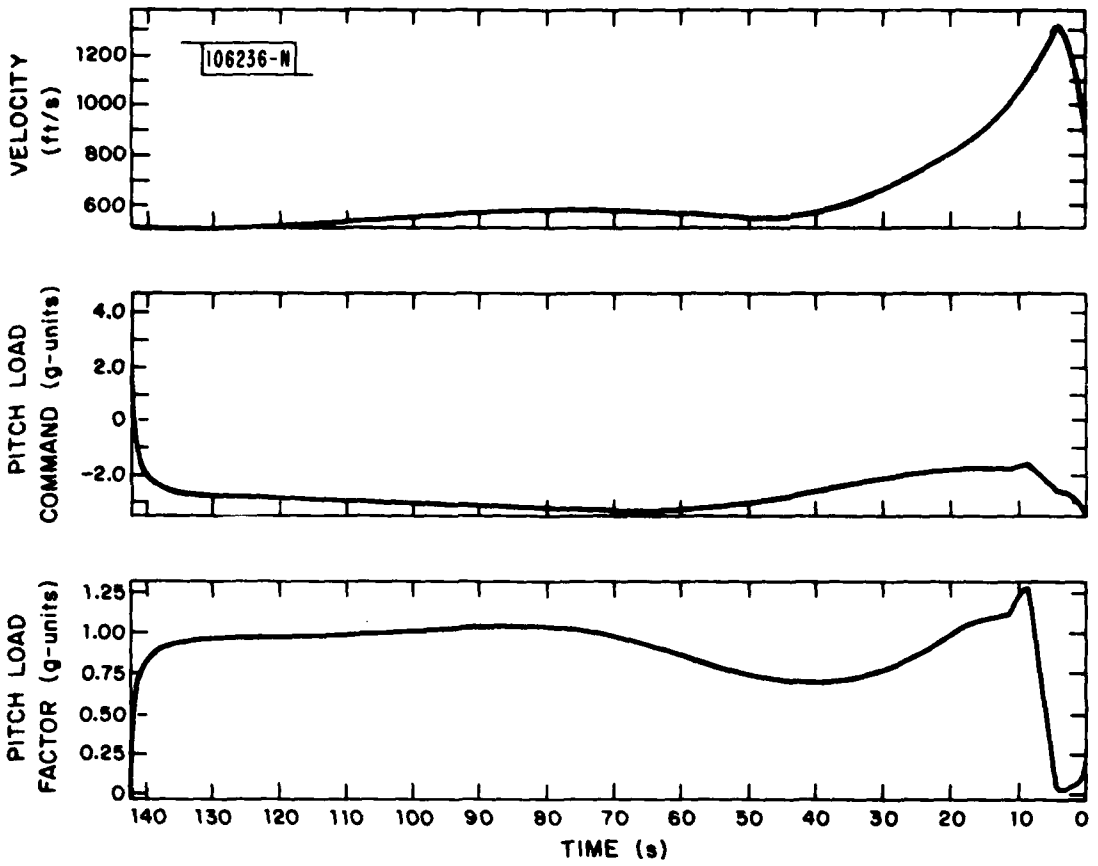

Fig. 4.1(b). Sample output for missile.

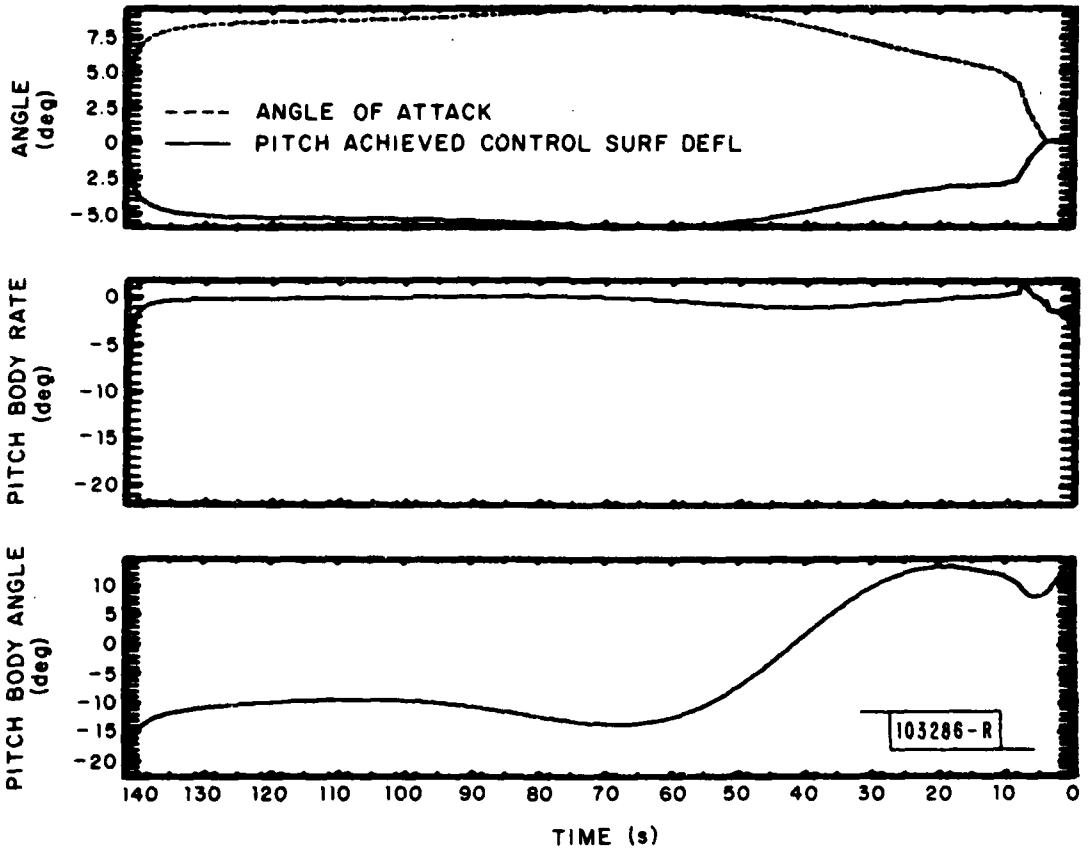

Fig. 4.1(c). Sample output for missile.

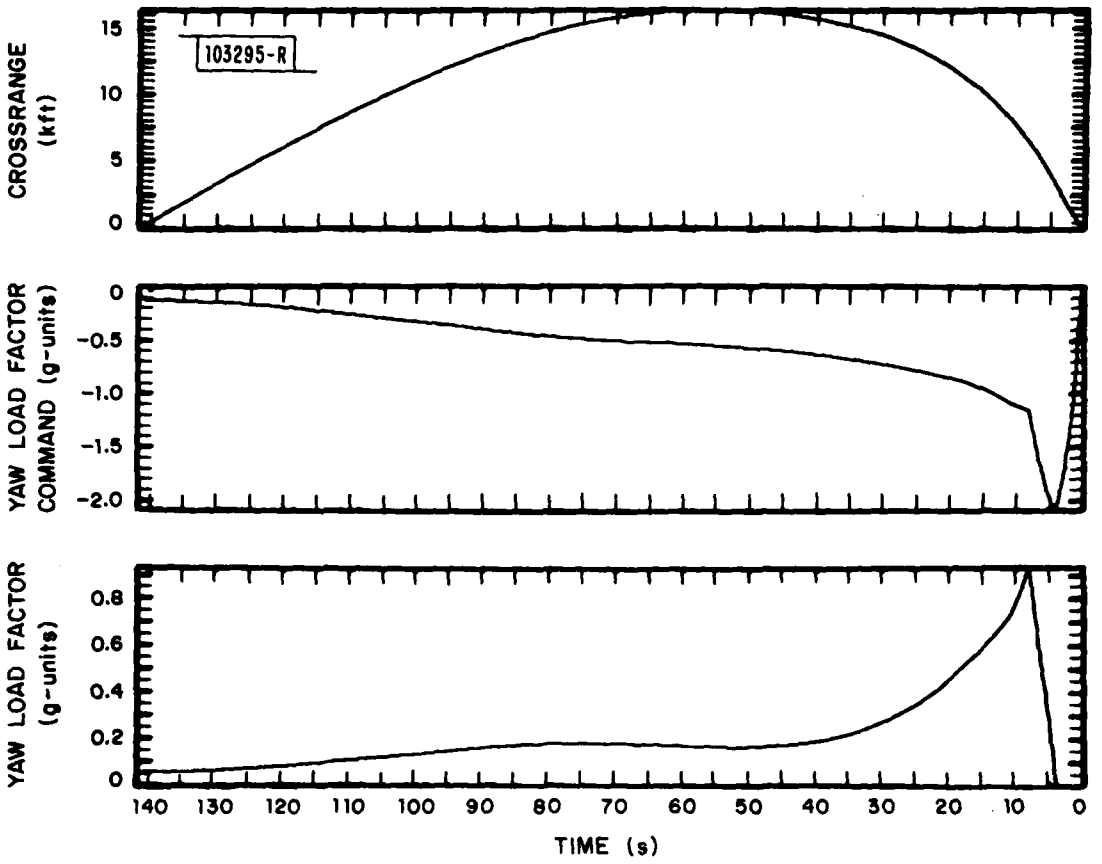

Fig. 4.1(d). Sample output for missile.

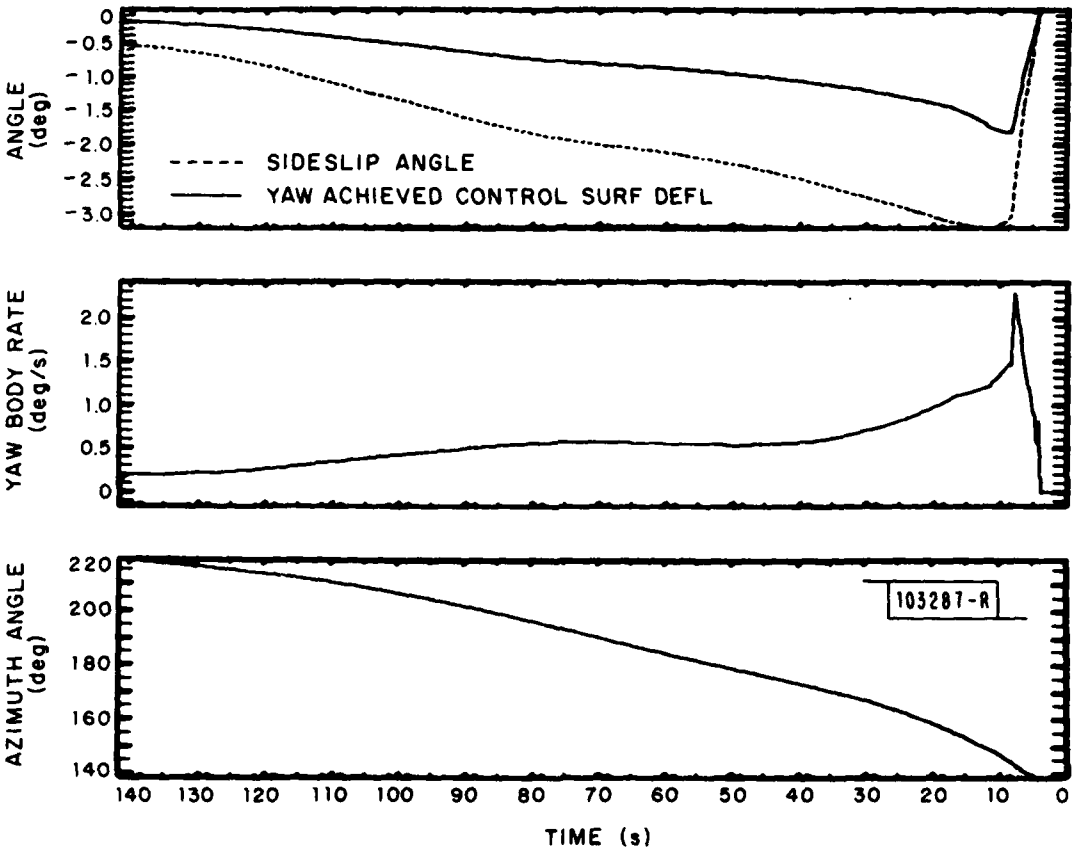

Fig. 4.1(e). Sample output for missile.

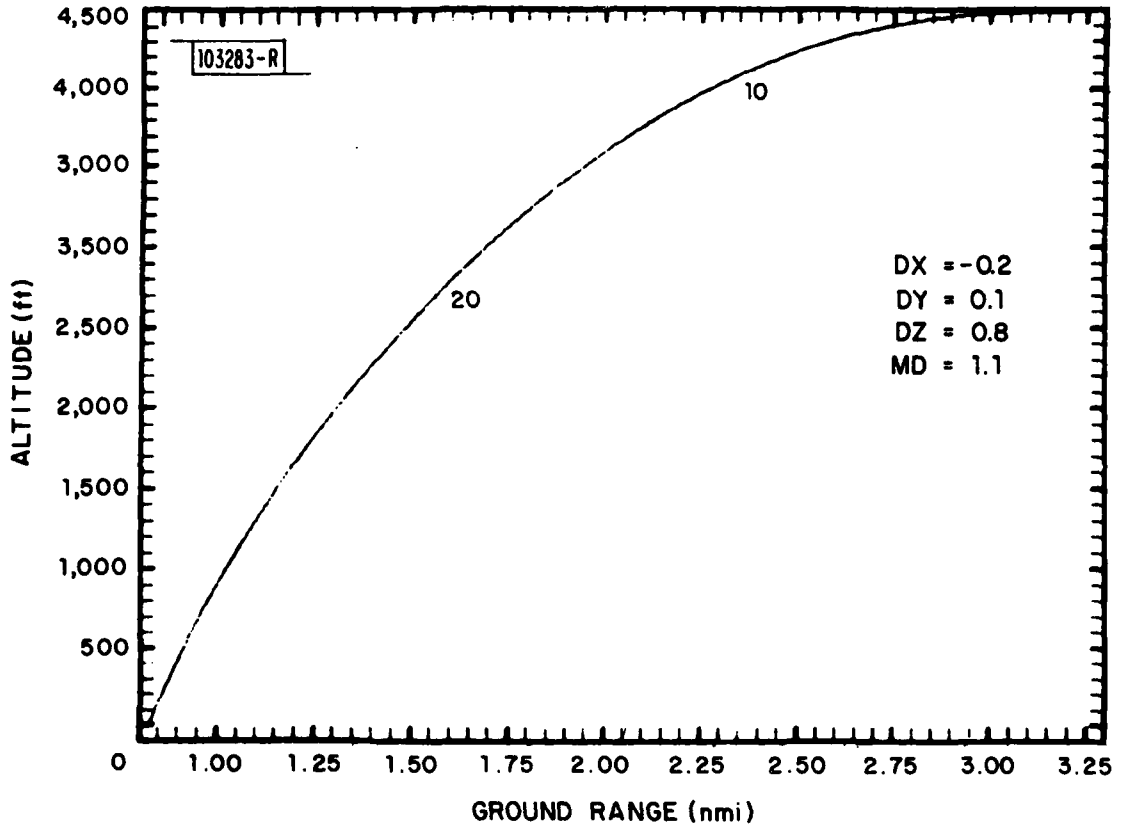

Fig. 4.2(a). Sample output for projectile.

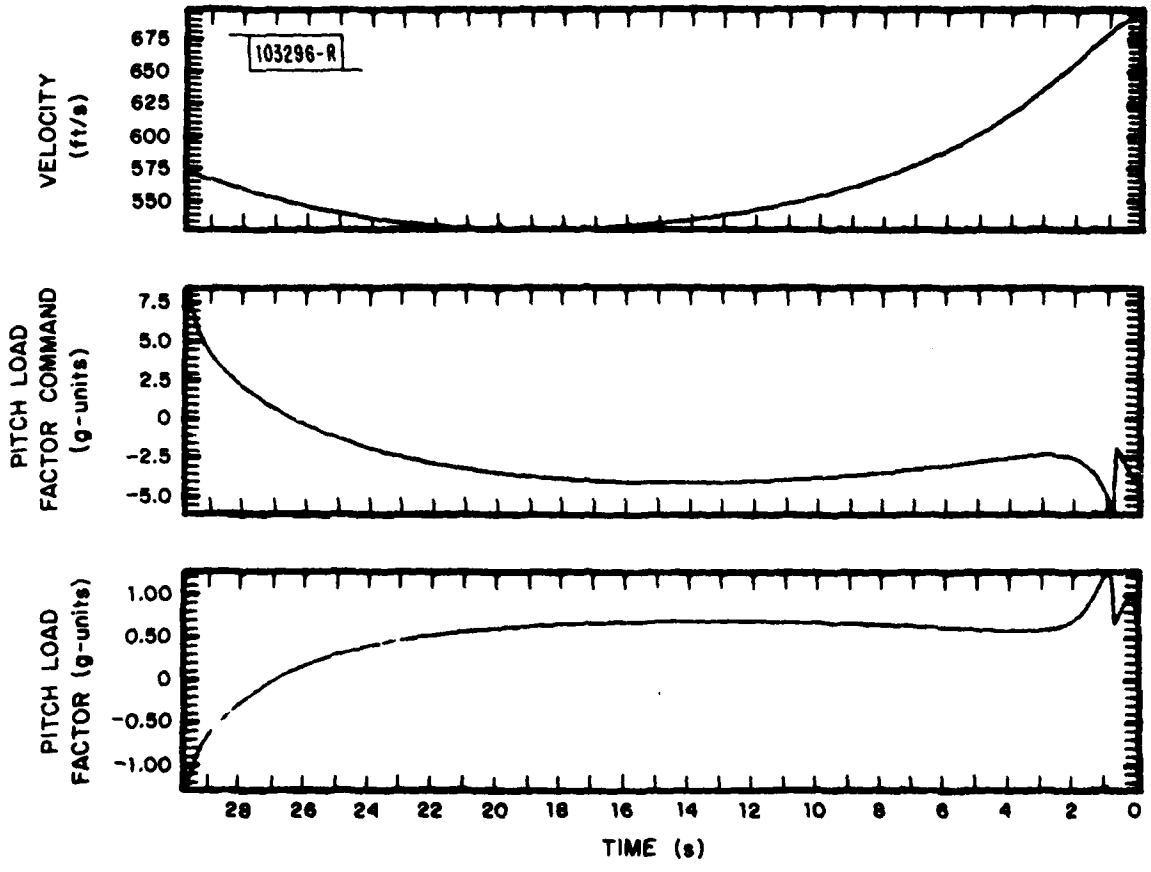

Fig. 4.2(b). Sample output for projectile.

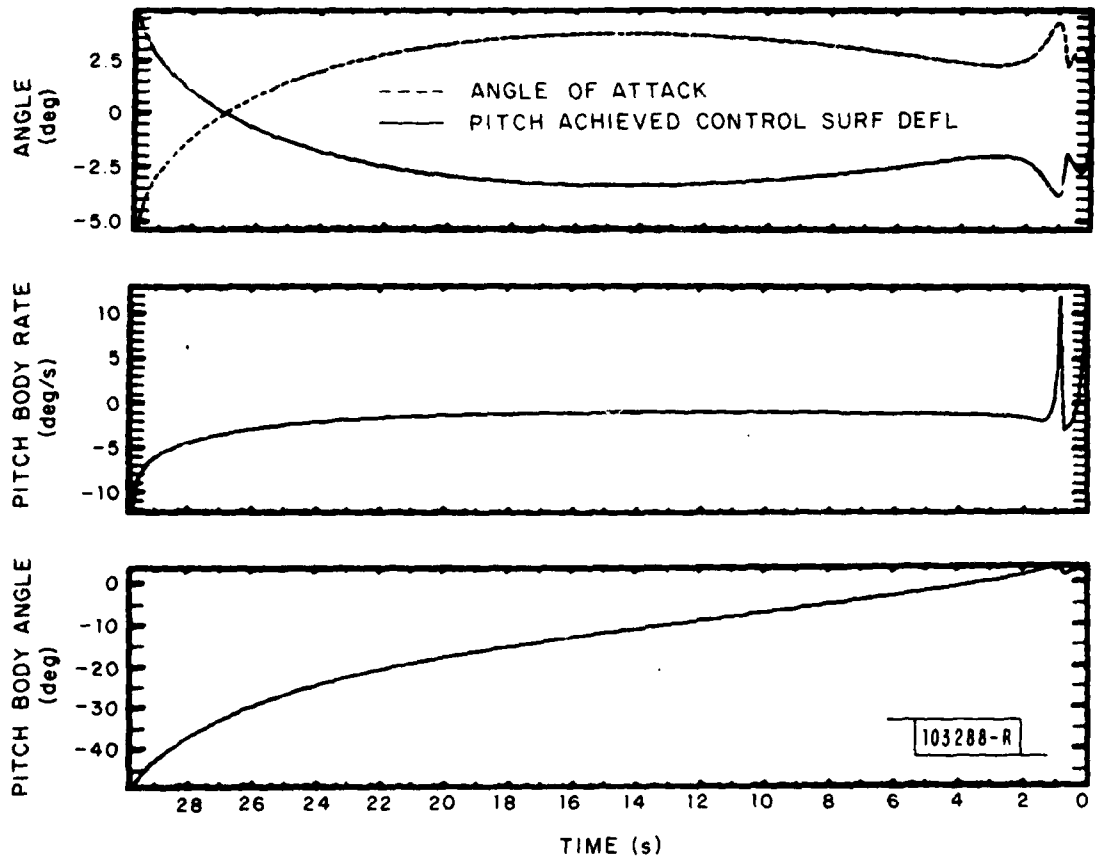

Fig. 4.2(c). Sample output for projectile.

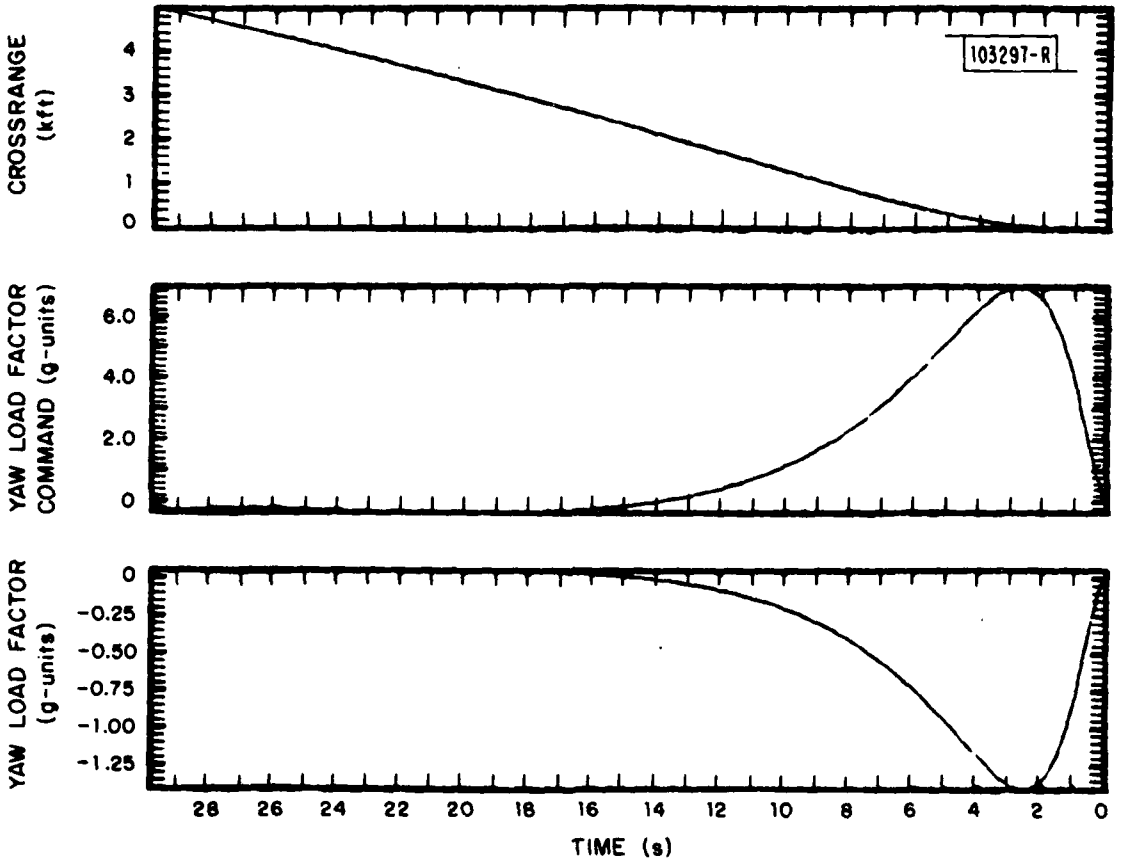

Fig. 4.2(d). Sample output for projectile.

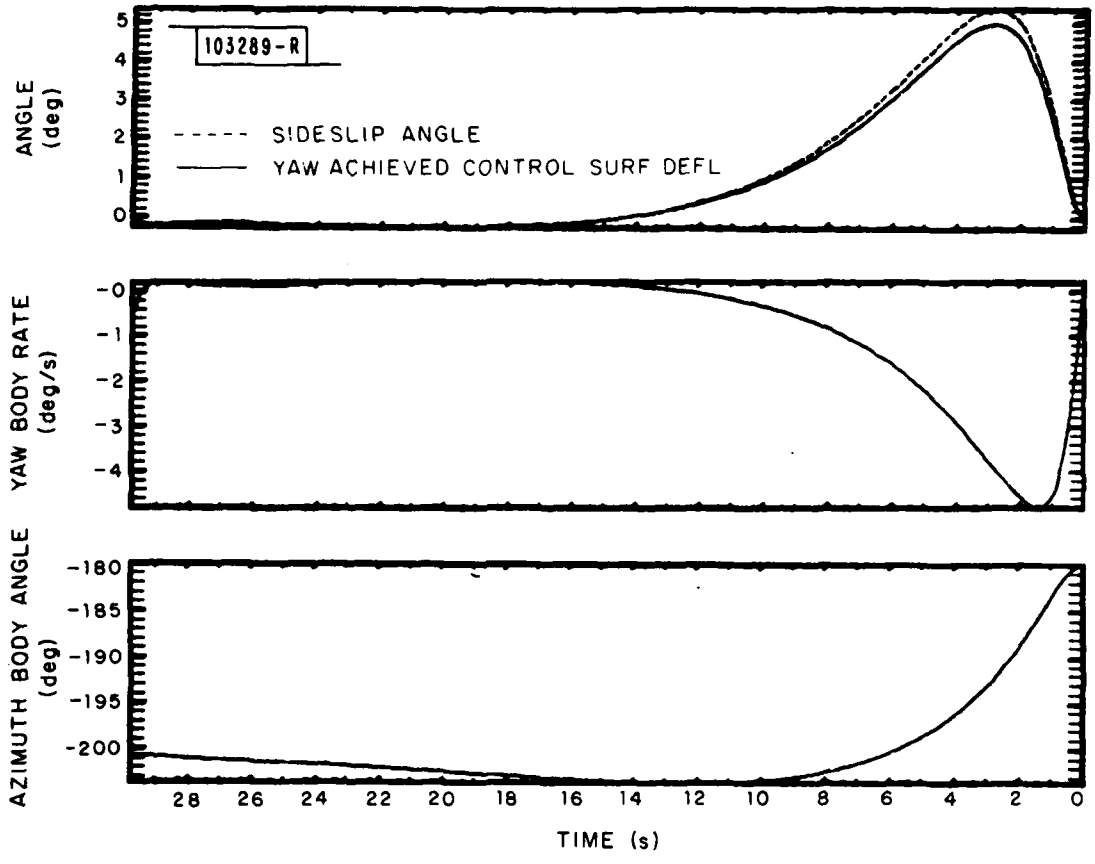

Fig. 4.2(e). Sample output for projectile.

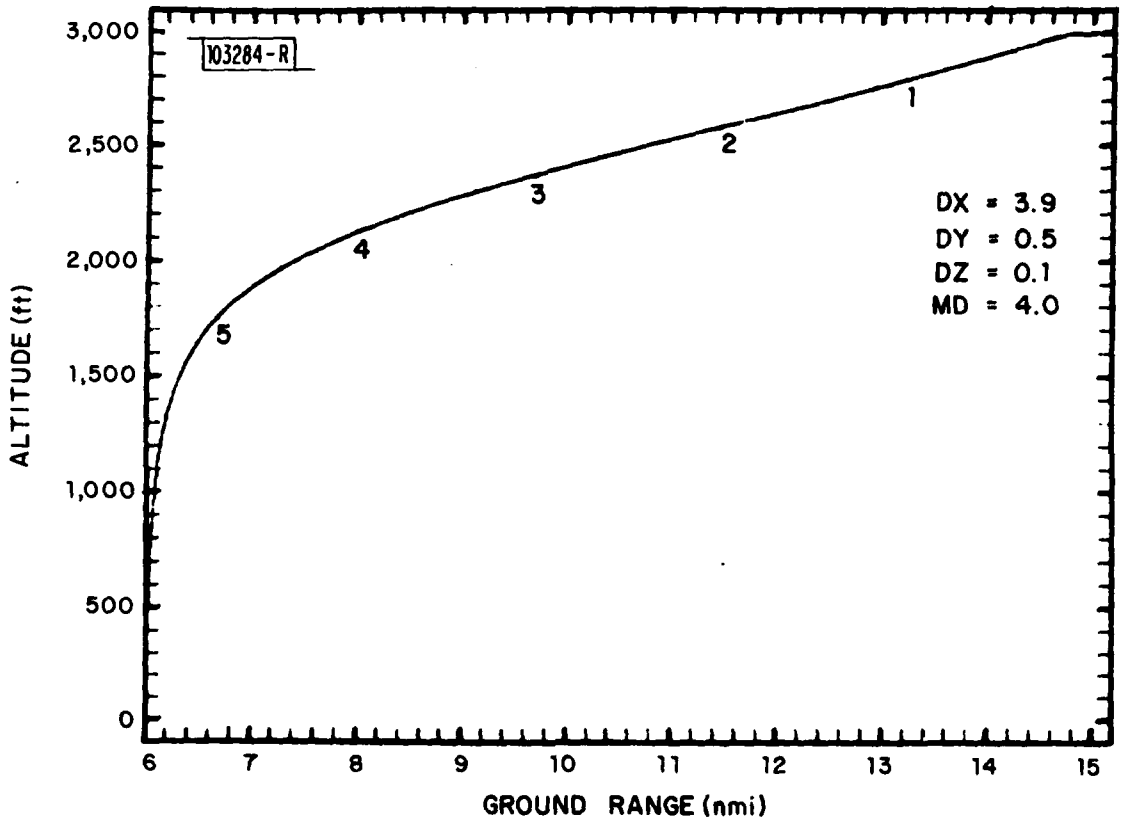

Fig. 4.3(a). Sample output for minidrone.

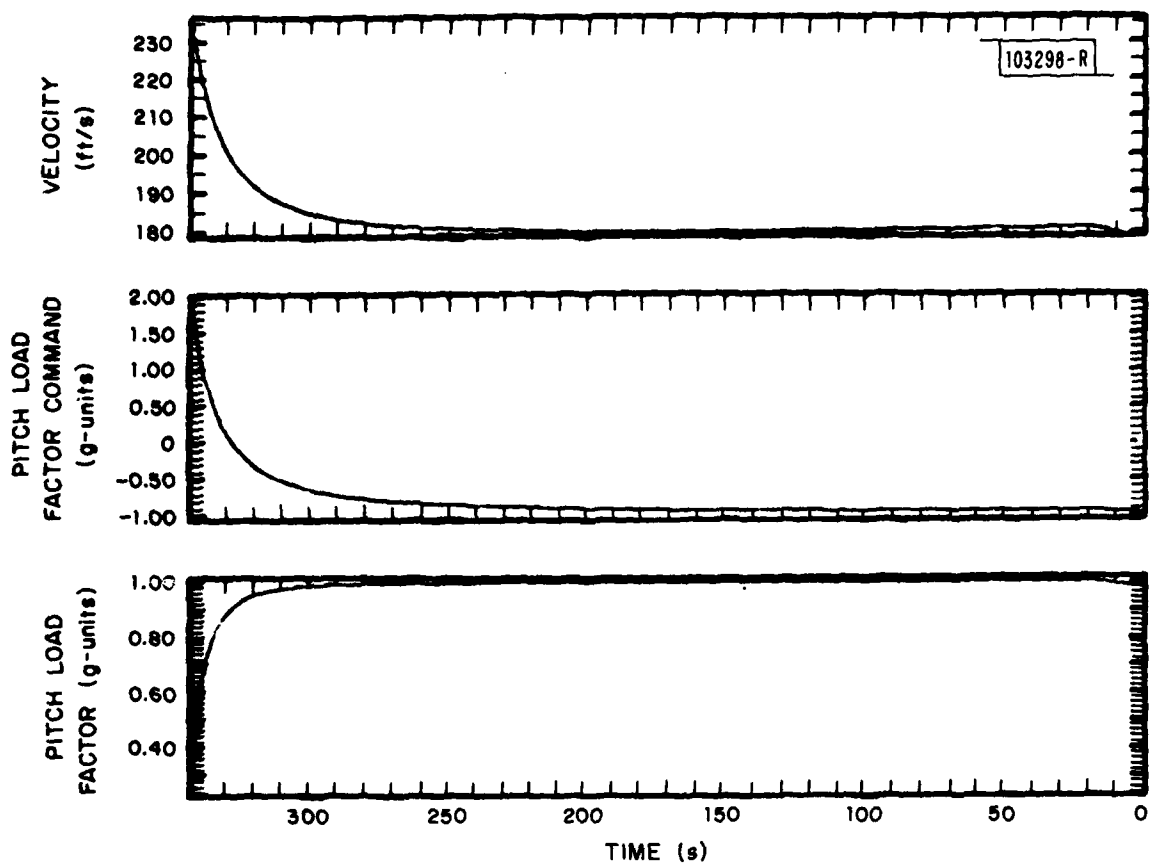

Fig. 4.3(b). Sample output for minidrone.

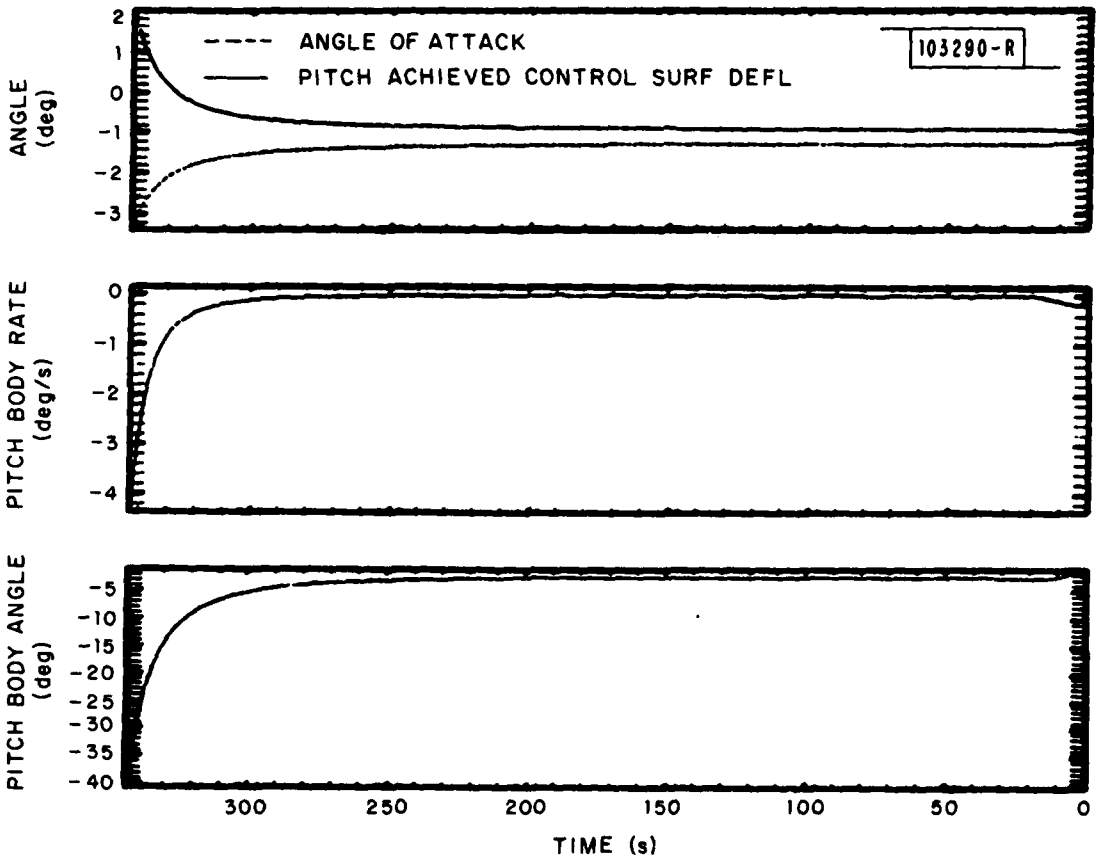

Fig. 4.3(c). Sample output for minidrone.

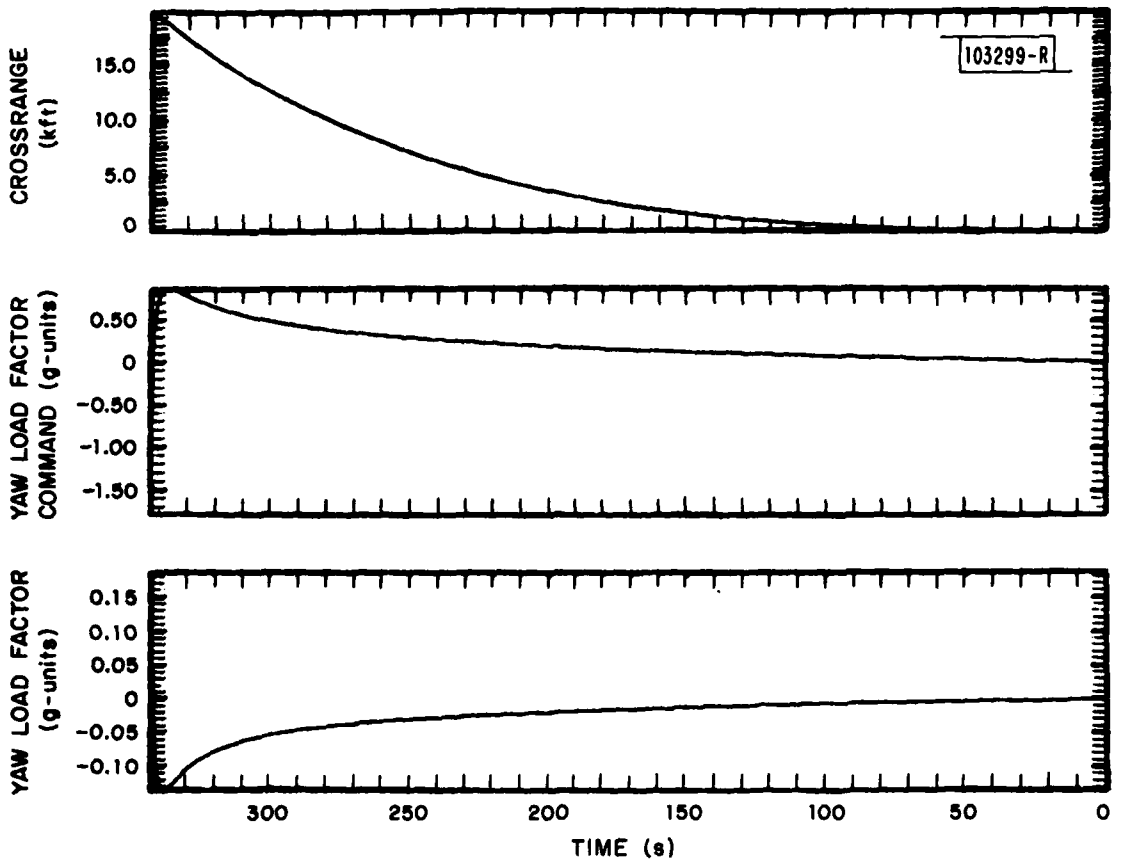

Fig. 4.3(d). Sample output for minidrone.

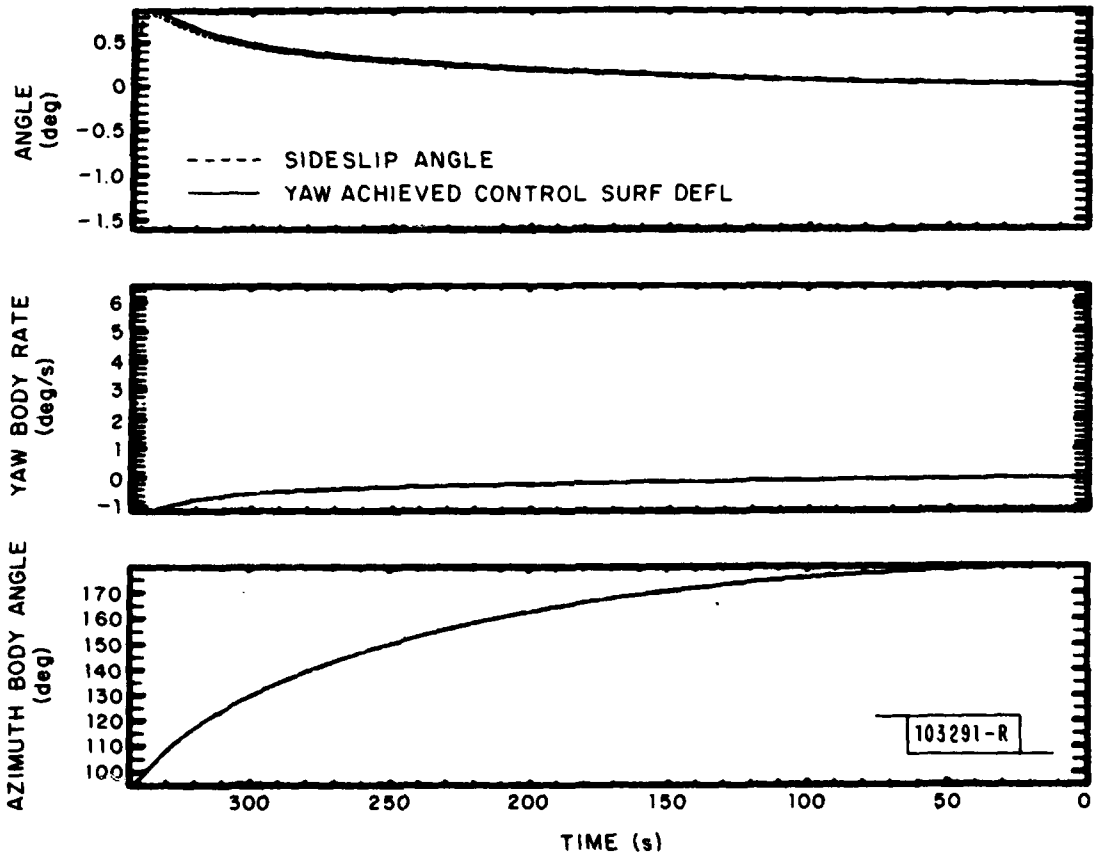

Fig. 4.3(e). Sample output for minidrone.

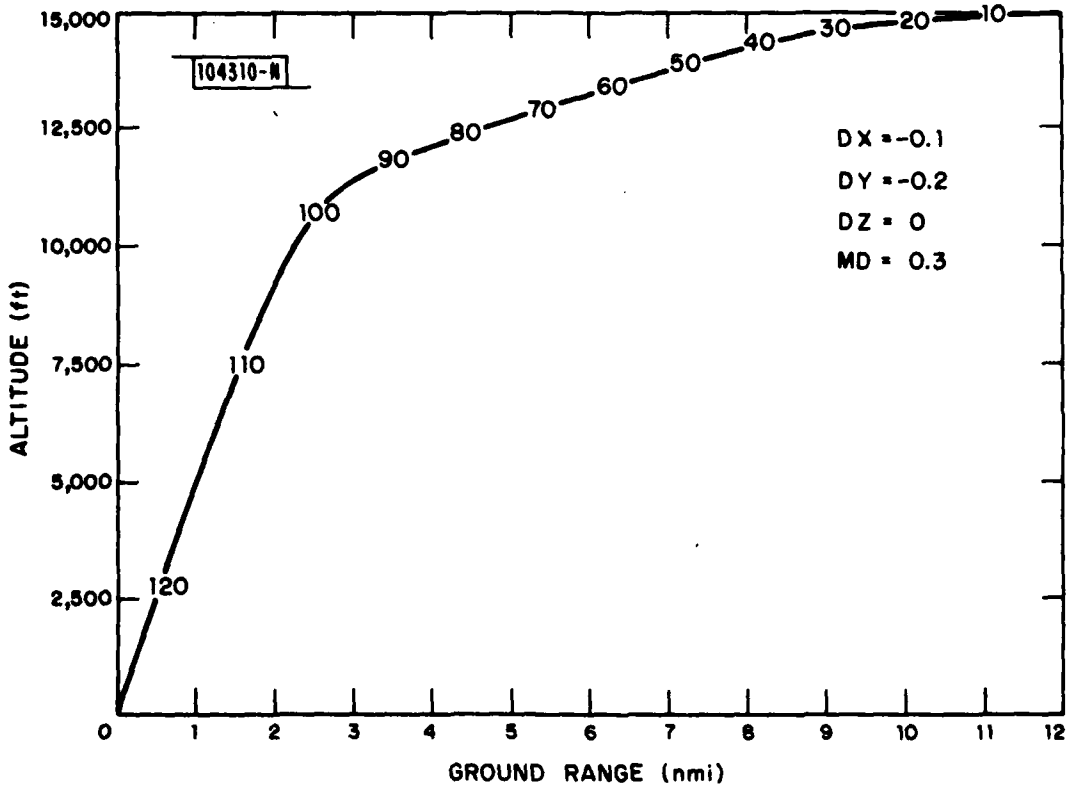

Fig. 4.4(a). Sample output for glide bomb.

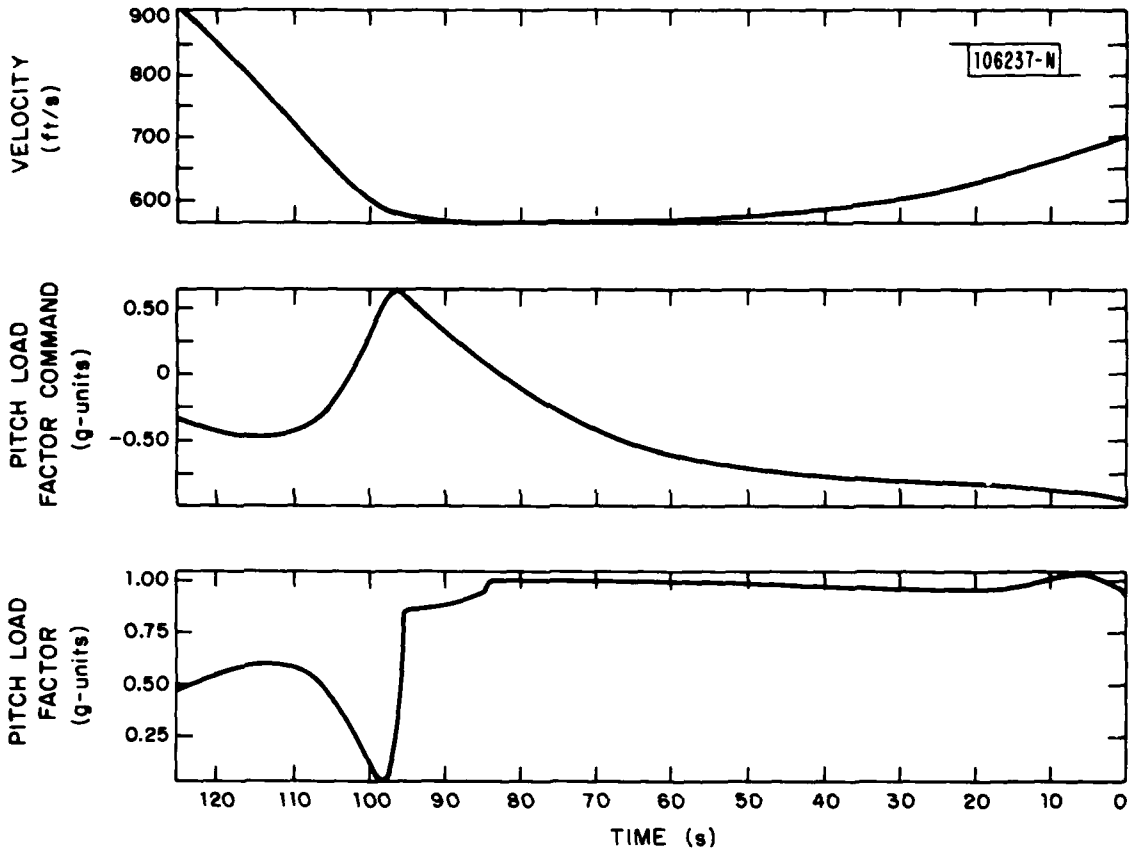

Fig. 4.4(b). Sample output for glide bomb.

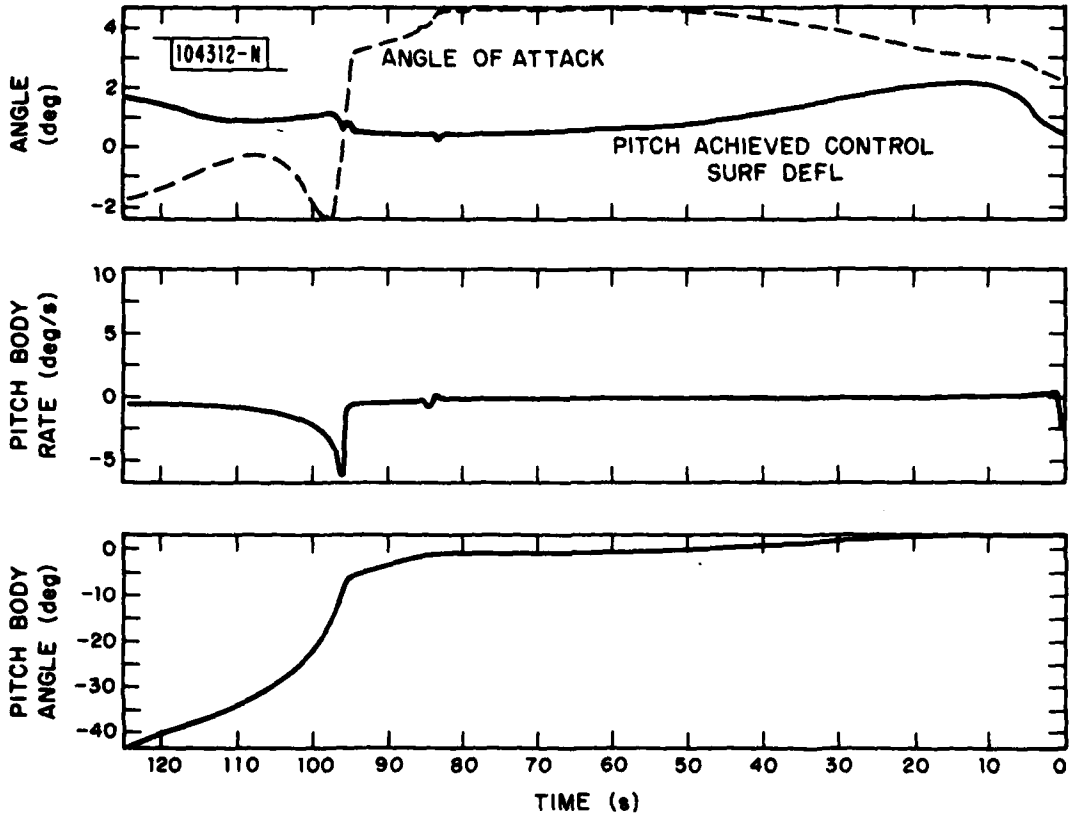

Fig. 4.4(c). Sample output for glide bomb.

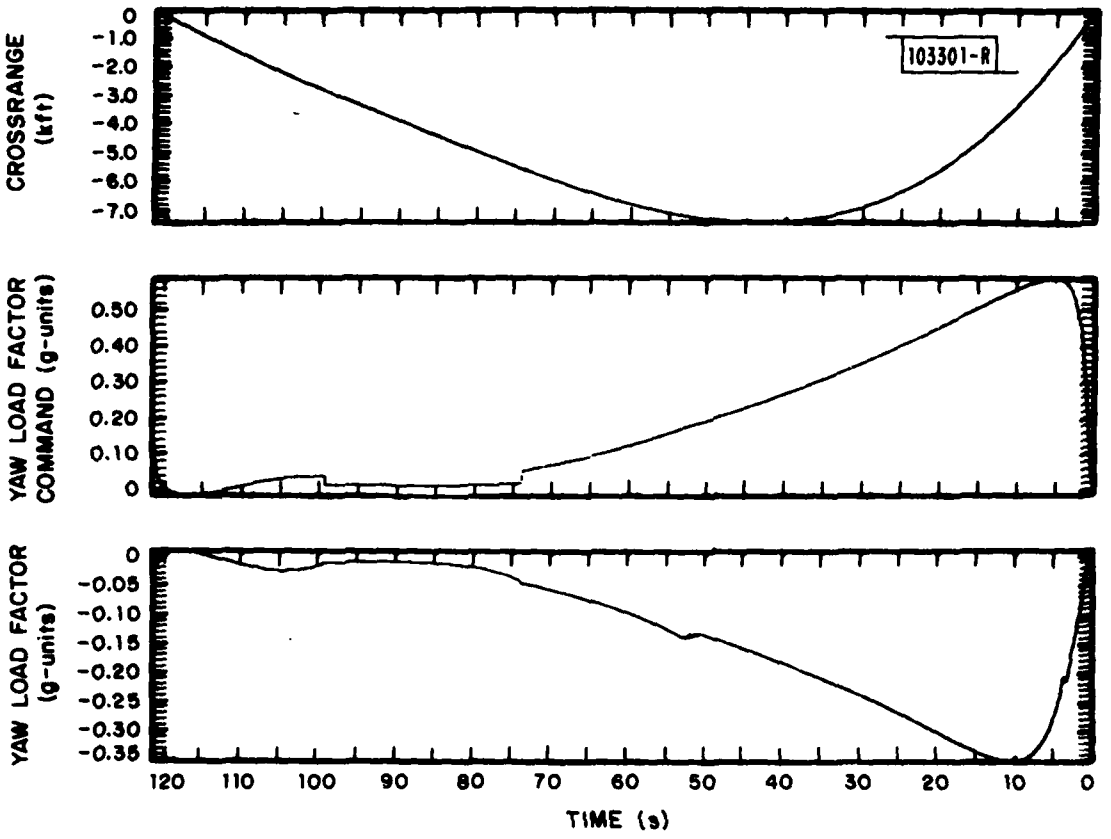

Fig. 4.4(d). Sample output for glode bomb.

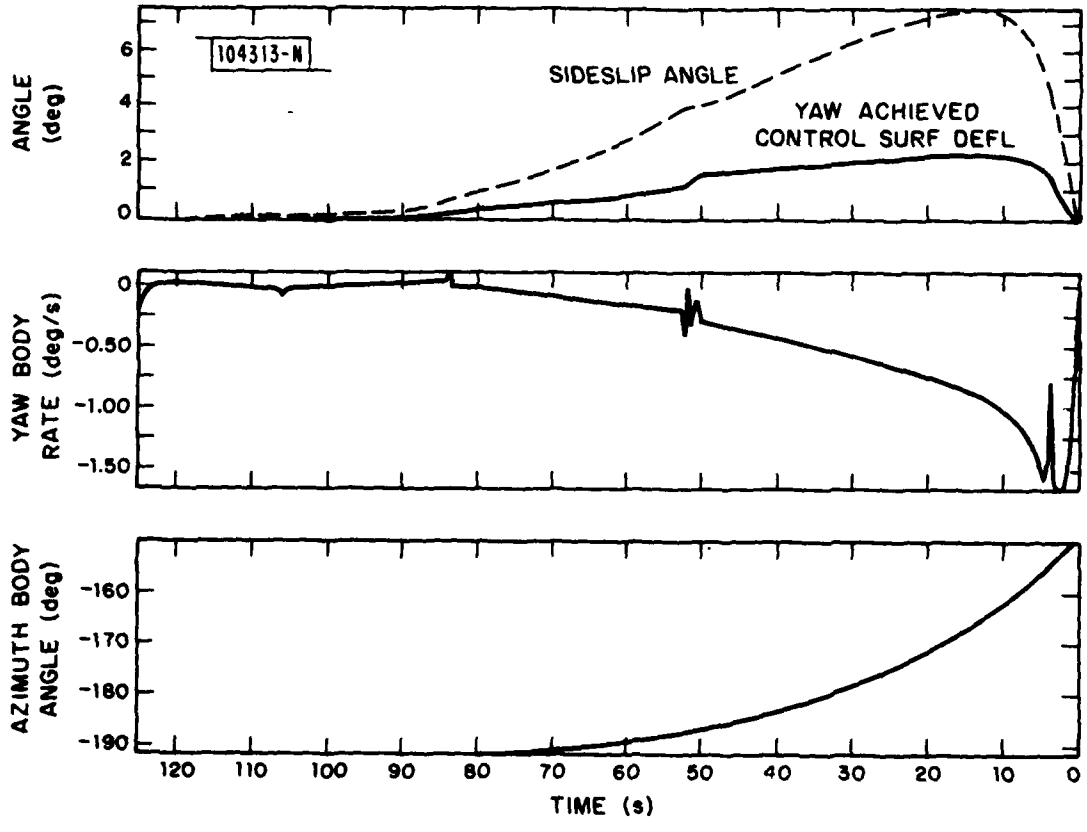

Fig. 4.4(e). Sample output for glide bomb.

For the projectile (4.2(b)), there is much less variation in the velocity from the starting value. The decrease indicates a drag of between $1/4$ and $1/2$ g which is, in part, balanced by the gravitational component. After about 20 seconds, the gravitational component becomes slightly larger than the drag component and the vehicle velocity increases slightly. The abrupt change in the load factor command at the beginning of the flight is the result of the vehicle coming to equilibrium when its control surface is released from a zero fixed position at the start of the flight. The command is a combination of the several inputs described in sections 2.5 and 3.3.

For the minidrone (Fig. 4.3(b)), the flight is fairly uneventful since it was assumed to be in straight and level flight at the start. The slight sagging of the trajectory is caused by the gyro bias error.

For the glide bomb (Fig. 4.4(b)), the velocity decays gradually from the initial condition of 700 ft/sec to about 570 ft/sec over a period of about 82 seconds. Then, the command of the vehicle is switched from angle-of-attack hold in pitch to gimbal angle hold, then about 15 seconds after this to the terminal mode of proportional navigation and the vehicle begins to dive, picking up speed until the final terminal velocity of about 900 ft/sec is reached. There is a substantial transient associated with the switching of the guidance mode as evidenced by the load factor response also shown in Fig. 4.4(b). It is appropriate to note that, although it is included on the center plot of 4.4(b), the commanded pitch load factor is not used until the terminal mode is switched in at about 97 seconds. As may be seen, the command level is about 0.65g at this time.

Figures 4.1(c) to 4.4(c) provide angle-of-attack and control surface deflection along with body pitch rate and angle. The transients in the projectile noted above are particularly noticeable in the body rate of Fig. 4.2(c). The switching transients for the glide bomb vehicle are quite noticeable in the response of all the variables in Fig. 4.4(c).

Figures 4.1(d), 4.2(d), 4.3(d), and 4.4(d) provide the cross range time history, as well as the command and achieved yaw factor. Figures 4.1(e), 4.2(e), 4.3(e), and 4.4(e) give the slide-slip angle and rudder control angle along with the yaw body rate and azimuth angle. The scheduled reduction in

the yaw gain during the pitch gimbal hold and terminal mode switching, as discussed in Section 2.5, can be clearly seen on the plots of Figures 4.4(d) and (e). Note the slight transients in the yaw body rate due to the switching as well as the abrupt change in the level of the commanded yaw load factor.

APPENDIX 1

MISSILE AERODYNAMIC DATA

The data presented in this Appendix is based upon reference 5. In terms of the tabular aerodynamic data, we define the following parameters:

$$\frac{C_N}{\alpha} = CN1 + CN2|\alpha| + CN3\ \alpha^2$$

$$\frac{C_Y}{\beta} = CN1 + CN2|\beta| + CN3\ \beta^2$$

$$\frac{C_m}{\alpha} = CM1 + CM2|\alpha| + CM3\ \alpha^2$$

$$\frac{C_n}{\beta} = CM1 + CM2|\beta| + CM3\ \beta^2$$

$$\frac{\Delta C_m}{\delta_E} = DCM1 + DCM2\ \alpha^2$$

$$\frac{\Delta C_n}{\delta_R} = DCM1 + DCM2\ \beta^2$$

and

$$C_x = CX1 + CX2(\alpha^2 + \beta^2) + CX3(\alpha^2 + \beta^2)^{1/2}\ (\delta_E^2 + \delta_R^2)^{1/2} + CX4(\delta_E^2 + \delta_R^2)$$

$$C_m = \left(\frac{C_m}{\alpha} - \frac{C_N}{\alpha}\frac{\Delta\ell}{\bar{C}_z}\right)\alpha + \frac{1}{r_o}\frac{\bar{C}_z}{2u}\ C_{M_Q}\ Q + \left(\frac{\Delta C_m}{\delta_E}\right)\left(1 - \frac{\Delta\ell}{\bar{C}_z}\right)\delta_E$$

$$C_n = \left(-\frac{C_m}{\beta} + \frac{C_Y}{\beta}\frac{\Delta\ell}{\bar{C}_Y}\right)\beta + \frac{1}{r_o}\frac{\bar{C}_Y}{2u}\ C_{M_R}\ R + \left(\frac{\Delta C_n}{\delta_R}\right)\left(1 - \frac{\Delta\ell}{\bar{C}_Y}\right)\delta_E$$

$$C_Y = -\left(\frac{\Delta C_n}{\delta_R}\right)\frac{1^*}{\ell_T}\ \delta_R + \left(\frac{C_Y}{\beta}\right)\beta$$

$$C_Z = \left(\frac{\Delta C_m}{\delta_E}\right)\frac{1^*}{\ell_T}\ \delta_E + \left(\frac{C_N}{\alpha}\right)\alpha$$

where

$C_{m_Q} = C_{M_R} = -573$

$\Delta\ell = 0.1166 - 0.1964t \qquad 0 \leq t \leq 0.5$

$\Delta\ell = 0.0184 - 0.0362\ (t - 0.5) \qquad 0.5 \leq t4$

$\Delta\ell = -0.1084 \qquad 4 \leq t$

$\ell_T = 3.5$

$\bar{C}_Y = \bar{C}_Z = 1.0$

and the needed aerodynamic parameters are given in Table A.1 as functions of Mach No. Note that α, β, δ_e, and δ_R are in degrees.

Since the inertial parameters are changing during the first four seconds of flight (after launch) the following are also needed for the equations of motion:

$m = 14.3478 - 1.3756t \qquad 0 \leq t \leq 0.5$

$m = 13.66 - 0.3714\ (t - 0.5) \qquad 0.5 \leq t \leq 4$

$m = 12.36 \qquad A \leq t$

$I_{YY} = I_{ZZ} = 64 - 3.8t \qquad 0 \leq t \leq 0.5$

$I_{YY} = I_{ZZ} = 62.1 - 1.0286\ (t - 0.5) \qquad 0.5 \leq t \leq 4$

$I_{YY} = I_{ZZ} = 58.5 \qquad 4 \leq t$

$T_{X/m} = 880 \qquad 0 \leq t \leq 0.5$

$T_{X/m} = 160 \qquad 0.5 \leq t \leq 4$

$T_{X/m} = 0 \qquad 4 < t$

TABLE A.1

MISSILE AERODYNAMIC DATA

	M	CX1	CX2	CX3	CX4
1	0.00	-3.25000E-01	1.80000E-04	-1.20000E-03	-3.50000E-04
2	0.30	-3.25000E-01	1.30000E-04	-1.20000E-03	-3.50000E-04
3	0.60	-3.25440E-01	1.25540E-04	-1.08000E-03	-3.39000E-04
4	0.80	-3.27557E-01	3.69160E-05	-8.97000E-04	-3.10000E-04
5	0.95	-5.50570E-01	1.21040E-04	-9.54000E-04	-3.11700E-04
6	1.14	-8.79650E-01	-1.21470E-04	-6.31000E-04	-2.00700E-04
7	1.30	-9.48900E-01	-2.04900E-04	-6.65500E-04	-3.72000E-04
8	1.80	-1.02000E+00	-2.60000E-04	-6.90000E-04	-4.00000E-04
9	2.00	-1.09000E+00	-3.20000E-04	-7.20000E-04	-5.00000E-04
10	2.50	-1.09000E+00	-3.20000E-04	-7.20000E-04	-5.00000E-04

	M	CN1	CN2	CN3
1	0.00	-1.90000E-01	-5.08500E-03	8.25000E-05
2	0.30	-1.90000E-01	-5.08550E-03	8.25000E-05
3	0.60	-1.92420E-01	-6.60250E-03	1.11400E-04
4	0.80	-1.94710E-01	-6.69130E-03	1.20690E-04
5	0.95	-2.01370E-01	-6.59920E-04	9.08910E-05
6	1.14	-2.07360E-01	-6.66600E-03	1.01500E-04
7	1.30	-2.10810E-01	-6.34160E-03	8.52700E-05
8	1.80	-1.90000E-01	-5.59500E-03	9.50000E-05
9	2.00	-1.83000E-01	-5.78000E-03	1.01000E-04
10	2.50	-1.83000E-01	-5.78000E-03	1.01000E-04

	M	CM1	CM2	CM3
1	0.00	-3.30000E-02	-8.30000E-03	1.25000E-04
2	0.30	-3.30000E-02	-8.30000E-03	1.25000E-04
3	0.60	-5.33280E-02	-8.78320E-03	2.04750E-04
4	0.80	-6.76040E-02	-9.02860E-03	2.51810E-04
5	0.95	-7.31390E-02	-1.13589E-02	3.87040E-04
6	1.14	-7.83710E-02	-6.51000E-03	2.47470E-04
7	1.30	-7.00940E-02	-9.55190E-03	3.13750E-04
8	1.80	-4.47500E-02	-9.22550E-03	2.70750E-04
9	2.00	-2.00000E-02	-9.57000E-03	2.50000E-04
10	2.50	-2.00000E-02	-9.57000E-03	2.50000E-04

	M	DCM1	DCM2
1	0.00	-1.62000E-01	-4.86000E-05
2	0.30	-1.62000E-01	-4.86000E-05
3	0.60	-2.10180E-01	-2.52900E-05
4	0.80	-2.32280E-01	-8.49800E-06
5	0.95	-2.12560E-01	-5.70160E-05
6	1.14	-1.64490E-01	-2.75700E-05
7	1.30	-1.44850E-01	-2.61600E-05
8	1.80	-1.20000E-01	-2.50000E-05
9	2.00	-1.00000E-01	-2.40000E-05
10	2.50	-1.00000E-01	-2.40000E-05

APPENDIX 2

PROJECTILE AERODYNAMIC DATA

The data presented in this appendix is based on references 6, 7, and 8. In terms of tabular aerodynamic data, we define the following parameters:

$$\frac{C_Z}{\alpha} = \text{CNALPHA} \qquad \frac{C_Y}{\beta} = \text{CNALPHA}$$

$$\frac{C_Z}{\delta_E} = \text{CNDELTA}\ (M,\ |\alpha|)$$

$$\frac{C_Y}{\delta_R} = -\text{CNDELTA}\ (M,\ |\beta|)$$

$$\frac{C_m}{\alpha} = \text{CMALPHA} \qquad \frac{C_n}{\beta} = -\text{CMALPHA}$$

$$\frac{C_m}{\delta_E} = \text{CMDELTA}\ (M,\ |\alpha|) \qquad \frac{C_n}{\delta_R} = \text{CMDELTA}\ (M,\ |\beta|)$$

$$C_x = -\ [\text{CXO} + \text{DELCX}\ (M,\ \alpha,\ \delta_E) + \text{DELCX}\ (M,\ \beta,\ \delta_R)]$$

and

$$C_Y = \frac{C_Y}{\beta}\ \beta + \frac{C_Y}{\delta_R}\ \delta_R$$

$$C_Z = \frac{C_Z}{\alpha}\ \alpha + \frac{C_Z}{\delta_E}\ \delta_E$$

$$C_m = \frac{C_m}{\alpha}\ \alpha + \frac{C_m}{\delta_E}\ \delta_E + \frac{1}{r_o}\ \frac{C_Z}{2U}\ C_{m_Q}\ Q$$

$$C_n = \frac{C_n}{\beta}\ \beta + \frac{C_n}{\delta_R}\ \delta_R + \frac{1}{r_o}\ \frac{C_Y}{2U}\ C_{n_R}\ R$$

and $C_{m_Q} = C_{n_R} = -155$. The needed aerodynamic parameters are given in Table A.2 as functions of M, α, β, δ_E and δ_R. Note that DELCX is a three dimensional table. All of the angular arguments are given in degrees.

TABLE A.2

PROJECTILE AERODYNAMIC DATA

	M	CX0	CNALPHA	CMALPHA
1	0.40	0.355	-0.340	-0.310
2	0.50	0.340	-0.342	-0.313
3	0.60	0.340	-0.348	-0.318
4	0.70	0.350	-0.360	-0.323
5	0.80	0.375	-0.385	-0.335
6	0.90	0.500	-0.425	-0.360
7	1.00	0.670	-0.440	-0.385

CNDELTA FUNCTION OF M & ABS VAL AOA

	M	AOA=0	AOA=5	AOA=10	AOA=15	AOA=20
1	0.40	-0.108	-0.110	-0.108	-0.045	-0.023
2	0.50	-0.110	-0.115	-0.110	-0.048	-0.025
3	0.60	-0.112	-0.120	-0.112	-0.050	-0.028
4	0.70	-0.117	-0.125	-0.117	-0.055	-0.030
5	0.80	-0.120	-0.130	-0.120	-0.060	-0.035
6	0.90	-0.130	-0.140	-0.130	-0.075	-0.050
7	1.00	-0.140	-0.148	-0.140	-0.100	-0.080

CMDELTA FUNCTION OF M & ABS VAL AOA

	M	AOA=0	AOA=5	AOA=10	AOA=15	AOA=20
1	0.40	-0.340	-0.330	-0.325	-0.120	-0.110
2	0.50	-0.348	-0.338	-0.328	-0.110	-0.100
3	0.60	-0.358	-0.345	-0.330	-0.100	-0.088
4	0.70	-0.370	-0.357	-0.340	-0.095	-0.075
5	0.80	-0.386	-0.370	-0.350	-0.105	-0.073
6	0.90	-0.413	-0.395	-0.365	-0.130	-0.088
7	1.00	-0.445	-0.422	-0.383	-0.163	-0.122

TABLE A.2 (cont'd)

PROJECTILE AERODYNAMIC DATA

DELCX FOR M=0.4
CONTROL SURFACE DEFLECTION

	AOA	-20	-15	-10	-5	0	5	10	15
1	-20	0.28	0.28	0.18	0.10	0.02	-0.07	-0.18	-0.19
2	-15	0.28	0.28	0.18	0.10	0.02	-0.07	-0.09	-0.03
3	-10	0.28	0.28	0.18	0.10	0.02	0.00	0.03	0.13
4	-5	0.24	0.24	0.16	0.03	0.00	0.02	0.10	0.21
5	0	0.52	0.30	0.15	0.06	0.00	0.06	0.18	0.22
6	5	0.41	0.21	0.10	0.02	0.00	0.03	0.16	0.24
7	10	0.26	0.13	0.03	0.00	0.02	0.10	0.18	0.28
8	15	0.05	-0.03	-0.09	-0.07	0.02	0.10	0.18	0.28
9	20	-0.10	-0.19	-0.18	-0.07	0.02	0.10	0.18	0.37

DELCX FOR M=0.8
CONTROL SURFACE DEFLECTION

	AOA	-20	-15	-10	-5	0	5	10	15
1	-20	0.37	0.25	0.10	0.00	-0.10	-0.18	-0.20	0.37
2	-15	0.37	0.25	0.10	0.00	-0.08	-0.11	-0.05	0.29
3	-10	0.29	0.20	0.09	0.00	-0.02	0.01	0.12	0.29
4	-5	0.29	0.20	0.09	0.00	0.03	0.11	0.25	0.40
5	0	0.30	0.16	0.07	0.00	0.05	0.16	0.22	0.37
6	5	0.25	0.11	0.03	0.00	0.09	0.20	0.29	0.30
7	10	0.12	0.01	-0.02	0.00	0.09	0.20	0.29	0.09
8	15	-0.05	-0.11	-0.08	0.00	0.10	0.25	0.37	-0.15
9	20	-0.20	-0.18	-0.10	0.00	0.10	0.25	0.37	0.45

DELCX FOR M=1.0
CONTROL SURFACE DEFLECTION

	AOA	-20	-15	-10	-5	0	5	10	15
1	-20	0.45	0.35	0.20	0.03	-0.13	-0.16	-0.13	0.40
2	-15	0.40	0.29	0.15	0.02	-0.05	-0.05	0.03	0.35
3	-10	0.35	0.24	0.08	0.01	0.01	0.05	0.16	0.30
4	-5	0.30	0.19	0.07	0.00	0.03	0.10	0.10	0.25
5	0	0.60	0.40	0.20	0.09	0.00	0.06	0.18	0.28
6	5	0.42	0.25	0.10	0.03	0.00	0.07	0.19	0.30
7	10	0.30	0.16	0.05	0.01	0.01	0.08	0.24	0.35
8	15	0.14	0.03	-0.05	-0.05	0.02	0.15	0.29	0.40
9	20	-0.06	-0.13	-0.16	-0.13	0.03	0.20	0.35	0.45

APPENDIX 3

MINIDRONE AERODYNAMIC DATA

The data presented in this appendix is based on reference 9. For the minidrone, the aerodynamic coefficients do not vary with Mach No. because of the relatively low speed of the vehicle.

$$C_m = C_{m_o} + C_{m_\alpha}\,\alpha + C_{m_{\delta E}}\,\delta_E + \frac{1}{r_o}\frac{\bar{C}_Z}{2U}\,C_{m_Q}\,Q$$

$$C_n = C_{n_\beta}\,\beta + C_{n_{\delta R}}\,\delta_R + \frac{1}{r_o}\frac{\bar{C}_Y}{2U}\,C_{n_R}\,R$$

$$C_L = C_{L_o} + C_{L_\alpha}\,\alpha + C_{L_\delta}\,\delta_E + \frac{1}{r_o}\frac{\bar{C}_Z}{2U}\,C_{L_Q}\,Q$$

$$C_Y' = C_{Y_\beta}\,\beta + C_{Y_\delta}\,\delta_R$$

$$C_o = C_{D_o} + \frac{C_L^{\,2}}{K_\alpha} + \frac{C_Y^{\,2}}{K_\beta}$$

$$C_X = -C_D\cos\alpha\cos\beta + C_L\sin\alpha + C_Y'\sin\beta$$

$$C_Y = -C_D\sin\beta - C_Y'\cos\beta$$

$$C_Z = -C_D\sin\alpha - C_L\cos\alpha$$

assuming small angles-of-attack and sideslip C_X, C_Y, C_Z can be written as

$$C_X = -C_D + \frac{1}{r_o}C_L\alpha + \frac{1}{r_o}C_Y'\beta$$

$$C_Y = \frac{1}{r_o}C_D\beta - C_Y'$$

$$C_Z = -\frac{1}{r_o} C_D\alpha - C_L$$

where all angles are in degrees. The coefficients are given as follows:

$C_{m_o} = -0.06$

$C_{m_\alpha} = -0.0300$

$C_{m_\delta} = -0.0223$

$C_{m_Q} = -17.0$

$C_{D_o} = 0.048$

$K_\alpha = 19.09$

$K_\beta = 6.03$

$C_{L_o} = 0.34$

$C_{L_\alpha} = 0.0960$

$C_{L_\delta} = 0.0062$

$C_{L_Q} = 7.0$

$C_{n_\beta} = 0.0140$

$C_{n_\delta} = -0.0140$

$C_{n_R} = -10.0$

$C'_{Y_\beta} = 0.0262$

$C'_{Y_\delta} = -0.0044$

The variation of the thrust with velocity is given as [8]:

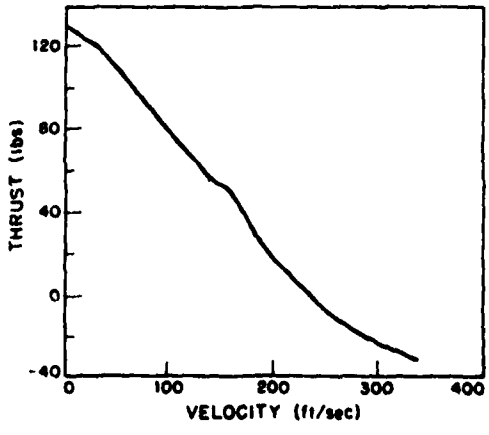

Fig. A.1. Thrust vs. velocity.

APPENDIX 4

GLIDE BOMB AERODYNAMIC DATA

The data presented in this appendix is based upon references 10, 11, 12. The aerodynamic coefficients are expressed as

$$C_X = -\{CXO(M, \alpha) + \frac{1}{r_o^2} [CXBETA\uparrow 2(M,\alpha)\ \beta^2 + CXDEL\uparrow 2(M)\ (\delta_E{}^2 + \delta_R{}^2)]\}$$

$$C_Y = C_{Y_\beta}\ \beta + CYDEL(M)\delta_R$$

$$C_Z = C_{Z_o} + C_{Z_\alpha}\ \alpha + CZDEL(M)\delta_E$$

$$C_m = C_{m_o}(M,\alpha) + DELCM(M,\alpha|\beta|) + CMDEL(M)\delta_E$$

$$C_n = DELC_n(M,\alpha,|\beta|)\ SGN(\beta) + C_nDEL(M)\delta_R$$

and $C_{Z_o} = -0.25$

$C_{Z_\alpha} = -0.10$

$C_{Y_\beta} = -0.029$

Table A.3 gives the aerodynamic parameters in these equations as functions of Mach No. and angles of attack and sideslip (α and β) as noted in the equations.

TABLE A.3

GLIDE BOMB AERODYNAMIC DATA

	M	CMDEL	CZDEL	CnDEL	CYDEL
1	0.50	-0.043600	-0.007000	-0.006300	0.0145000
2	0.70	-0.038400	-0.007900	-0.006100	0.0148000
3	0.90	-0.040100	-0.009800	-0.006800	0.0140000
4	1.10	-0.031400	-0.008200	-0.004400	0.0105000
5	1.30	-0.024400	-0.006500	-0.003100	0.0079000

CmO AS A FUNCTION OF M & ALPHA

	M	ALP=-15	ALP=-10	ALP=-5	ALP=0	ALP=5	ALP=10
1	0.50	0.063000	0.068000	0.062500	0.0343000	0.009300	0.042300
2	0.70	0.070200	0.080000	0.058400	0.0306000	0.010100	0.054500
3	0.90	0.176000	0.183000	0.102300	0.0150000	-0.081800	-0.079500
4	1.10	0.371000	0.290000	0.150500	-0.0200000	-0.315000	-0.566000
5	1.30	0.280000	0.259000	0.079200	-0.0920000	-0.320500	-0.588000

CXO AS A FUNCTION OF M & ALPHA

	M	ALP=-15	ALP=-10	ALP=-5	ALP=0	ALP=5	ALP=10
1	0.50	0.033000	0.029000	0.039800	0.0566000	0.008200	0.062800
2	0.70	0.044200	0.034000	0.040400	0.0570000	0.008200	0.047800
3	0.90	0.069600	0.048500	0.060100	0.0855000	0.086100	0.082000
4	1.10	0.153000	0.159800	0.154700	0.1248000	0.142600	0.151500
5	1.30	0.120200	0.135900	0.149100	0.1588000	0.162000	0.160100

CX BETA↑2 AS A FUNCTION OF M & ALPHA

	M	ALP=-15	ALP=-10	ALP=-5	ALP=0	ALP=5	ALP=10
1	0.50	0.050000	0.050000	-0.154000	-0.7860000	-0.122000	-0.120000
2	0.70	0.270000	0.270000	-0.120000	-0.9100000	-0.168000	-0.168000
3	0.90	0.560000	0.560000	-0.320000	-0.6800000	-0.370000	-0.370000
4	1.10	-0.070000	-0.070000	-0.240000	-0.3800000	-0.290000	-0.290000
5	1.30	0.000000	0.000000	-0.072000	-0.2000000	-0.188000	-0.188000

CX DEL↑2 AS A FUNCTION OF M

	M	
1	0.50	0.515000
2	0.70	0.742000
3	0.90	1.069000
4	1.10	0.897000
5	1.30	0.672000

TABLE A.3 (cont'd)

GLIDE BOMB AERODYNAMIC DATA

DELCM VS M & ABS(BETA) FOR ALPHA=-15

	M	BETA=0	BETA=4	BETA=8	BETA=12
1	0.50	0.000000	0.019300	-0.004200	0.0278000
2	0.70	0.000000	-0.012800	-0.027500	-0.0132000
3	0.90	0.000000	-0.035800	-0.210600	-0.1684000
4	1.10	0.000000	-0.036900	-0.090700	-0.0925000
5	1.30	0.000000	-0.013100	-0.040700	-0.0306000

DELCM VS M & ABS(BETA) FOR ALPHA=-10

	M	BETA=0	BETA=4	BETA=8	BETA=12
1	0.50	0.000000	0.023000	0.039700	0.0439000
2	0.70	0.000000	0.008400	0.026600	0.0181000
3	0.90	0.000000	0.004000	-0.049200	-0.0595000
4	1.10	0.000000	-0.007500	-0.009900	0.0153000
5	1.30	0.000000	-0.002900	0.006700	0.0189000

DELCM VS M & ABS(BETA) FOR ALPHA=-5

	M	BETA=0	BETA=4	BETA=8	BETA=12
1	0.50	0.000000	0.026700	0.083600	0.0600000
2	0.70	0.000000	0.030000	0.080600	0.0494000
3	0.90	0.000000	0.043800	0.112200	0.0494000
4	1.10	0.000000	0.021900	0.070900	0.0325000
5	1.30	0.000000	0.007300	0.054100	0.0684000

DELCM VS M & ABS(BETA) FOR ALPHA= 0

	M	BETA=0	BETA=4	BETA=8	BETA=12
1	0.50	0.000000	0.018800	0.076000	0.0960000
2	0.70	0.000000	0.023800	0.088100	0.1027000
3	0.90	0.000000	0.021000	0.125800	0.1427000
4	1.10	0.000000	0.041700	0.131800	0.1662000
5	1.30	0.000000	0.007300	0.017500	0.0463000

DELCM VS M & ABS(BETA) FOR ALPHA= 5

	M	BETA=0	BETA=4	BETA=8	BETA=12
1	0.50	0.000000	0.017100	0.039900	0.0618000
2	0.70	0.000000	0.019000	0.050100	0.1067000
3	0.90	0.000000	0.059500	0.129800	0.2102000
4	1.10	0.000000	0.031300	0.088300	0.1961000
5	1.30	0.000000	-0.004200	-0.041000	-0.0034000

DELCM VS M & ABS(BETA) FOR ALPHA= 10

	M	BETA=0	BETA=4	BETA=8	BETA=12
1	0.50	0.000000	0.010800	-0.004300	0.0225000
2	0.70	0.000000	0.022500	-0.005700	0.0699000
3	0.90	0.000000	0.077300	0.127900	0.2542000
4	1.10	0.000000	0.026100	0.064800	0.2339000
5	1.30	0.000000	0.036400	0.111800	0.1583000

TABLE A.3 (cont'd)

GLIDE BOMB AERODYNAMIC DATA

DELCn VS M & ABS(BETA) FOR ALPHA=-15

	M	BETA=0	BETA=4	BETA=8	BETA=12
1	0.50	0.000000	0.003000	0.001000	0.0000000
2	0.70	0.000000	0.003000	0.002600	0.0024000
3	0.90	0.000000	0.010000	0.006000	0.0030000
4	1.10	0.000000	0.005000	0.006000	0.0120000
5	1.30	0.000000	0.002000	0.003000	0.0050000

DELCn VS M & ABS(BETA) FOR ALPHA=-10

	M	BETA=0	BETA=4	BETA=8	BETA=12
1	0.50	0.000000	0.005000	0.003500	0.0020000
2	0.70	0.000000	0.005000	0.006700	0.0060000
3	0.90	0.000000	0.013000	0.011000	0.0110000
4	1.10	0.000000	0.005500	0.009000	0.0150000
5	1.30	0.000000	0.002500	0.002500	0.0085000

DELCn VS M & ABS(BETA) FOR ALPHA=-5

	M	BETA=0	BETA=4	BETA=8	BETA=12
1	0.50	0.000000	0.006500	0.008000	0.0130000
2	0.70	0.000000	0.007800	0.009600	0.0062000
3	0.90	0.000000	0.015500	0.019000	0.0210000
4	1.10	0.000000	0.008500	0.011000	0.0160000
5	1.30	0.000000	0.006000	0.010000	0.0180000

DELCn VS M & ABS(BETA) FOR ALPHA= 0

	M	BETA=0	BETA=4	BETA=8	BETA=12
1	0.50	0.000000	0.007000	0.012500	0.0295000
2	0.70	0.000000	0.008000	0.015000	0.0330000
3	0.90	0.000000	0.012000	0.021000	0.0410000
4	1.10	0.000000	0.015000	0.015000	0.0250000
5	1.30	0.000000	0.005500	0.014500	0.0275000

DELCn VS M & ABS(BETA) FOR ALPHA= 5

	M	BETA=0	BETA=4	BETA=8	BETA=12
1	0.50	0.000000	0.009500	0.021000	0.0355000
2	0.70	0.000000	0.013000	0.021000	0.0391000
3	0.90	0.000000	0.013500	0.024000	0.0420000
4	1.10	0.000000	0.013000	0.024000	0.0340000
5	1.30	0.000000	0.004500	0.014500	0.0295000

DELCn VS M & ABS(BETA) FOR ALPHA= 10

	M	BETA=0	BETA=4	BETA=8	BETA=12
1	0.50	0.000000	0.010300	0.024300	0.0430000
2	0.70	0.000000	0.010400	0.026500	0.0428000
3	0.90	0.000000	0.013500	0.024000	0.0420000
4	1.10	0.000000	0.016800	0.030700	0.0423000
5	1.30	0.000000	0.004500	0.014500	0.0295000

REFERENCES

1. I.G. Stiglitz, "A Precision Guided Weapons System Concept for Command and Control Countermeasures," Project Report TST-40, Lincoln Laboratory, M.I.T. (26 July 1979).

2. P.H. Morrison, "Guidance and Control of a Cannon Launched Projectile," AIAA Guidance and Control Conference (1976).

3. H. Ashley, Engineering Analysis of Flight Vehicles, (Addison-Wesley, Reading, MA, 1974).

4. J. Roskam, "Flight Dynamics of Rigid and Elastic Airplanes," Roskam Aviation and Engineering Corportation, Lawrence, Kansas (1972).

5. C. Terrazas, Private Communication, Hughes Aircraft.

6. R.A. Nulk, H.L. Pastrick and P.A. Morrison, "Copperhead Semi-Active Laser Guidance System Development," AIAA Guidance and Control Conference, 1978.

7. P.H. Morrison, "A Lesson Learned About Cannon Launched Guidance Projectiles," AIAA Guidance and Control Conference, 1978.

8. H.E. Hudgins, "Aerodynamics, Dimenstions, Inertial Properties and Performance of Artillery Projectiles," Picatinny Arsenal, No. 4911 (January 1977).

9. R. D'Amato, J. Capon, "Digital Simulation of a Mini Drone," Project Report TST-29, Lincoln Laboratory, M.I.T. (1 February 1979), DDC AD-B036934-L.

10. "GBU-15 PWW/WCU Development," Program Report No. GBU 1190-1A, Revision A, Hughes Aircrft Company (1 April 1977).

11. D.F. Cupitt, "GBU-15 PWW.WCU Development," Program Report No. GBU 1151-1A Revision A, Hughes Aircraft Company (28 January 1977).

12. "GBU-15 PWW/WCU Development," Program Report No. GBU 1151-1A Revision A, Hughes Aircraft Company (28 January 1977).

13. C.E. Mueller, R.K. Phelps and R. Scheidenhelm, "Tactical Guidance Requirements for Strapdown Inertial," NAECON 77 Record.

UNCLASSIFIED

SECURITY CLASSIFICATION OF THIS PAGE (When Data Entered)

19 REPORT DOCUMENTATION PAGE		READ INSTRUCTIONS BEFORE COMPLETING FORM
1. REPORT NUMBER 18 ESD-TR-80-170	2. GOVT ACCESSION NO. AD-A096	3. RECIPIENT'S CATALOG NUMBER 050
4. TITLE (and Subtitle) 6 Digital Simulation Models of Candidate Tactical Weapons		5. TYPE OF REPORT & PERIOD COVERED 9 Project Report
		6. PERFORMING ORG. REPORT NUMBER Project Report TST-45
7. AUTHOR(s) 10 Richard D'Amato Christopher M. Sorrentino Jack Capon		8. CONTRACT OR GRANT NUMBER(s) 15 F19628-80-C-0002
9. PERFORMING ORGANIZATION NAME AND ADDRESS Lincoln Laboratory, M.I.T. P.O. Box 73 Lexington, MA 02173		10. PROGRAM ELEMENT, PROJECT, TASK AREA & WORK UNIT NUMBERS Program Element No. 63601F 16 Project No. 670B
11. CONTROLLING OFFICE NAME AND ADDRESS Air Force Systems Command, USAF Andrews AFB Washington, DC 20331		12. REPORT DATE 11 9 September 1980
		13. NUMBER OF PAGES 82 (12) 84
14. MONITORING AGENCY NAME & ADDRESS (if different from Controlling Office) Electronic Systems Division (14) TST-45 Hanscom AFB Bedford, MA 01731		15. SECURITY CLASS. (of this report) Unclassified
		15a. DECLASSIFICATION DOWNGRADING SCHEDULE

16. DISTRIBUTION STATEMENT (of this Report)

Approved for public release; distribution unlimited.

17. DISTRIBUTION STATEMENT (of the abstract entered in Block 20, if different from Report)

18. SUPPLEMENTARY NOTES

None

19. KEY WORDS (Continue on reverse side if necessary and identify by block number)

degree of freedom
digital simulation
tactical weapons
emitter homing
closed loop

20. ABSTRACT (Continue on reverse side if necessary and identify by block number)

A five degree-of-freedom simulation has been constructed for each of four candidate tactical weapons for use in a program to develop/evaluate new techniques for emitter homing. The vehicle types include a powered missile, a projectile, a minidrone, and a glide bomb. The roll degree-of-freedom was eliminated from the simulation on the basis that each vehicle is stabilized in roll with low roll rates. The report provides detailed descriptions of the simulations including the aerodynamic and autopilot models, along with the numerical procedures used. Typical responses of the closed loop homing performance are given for each vehicle.

DD FORM 1 JAN 73 1473 EDITION OF 1 NOV 65 IS OBSOLETE

UNCLASSIFIED 207650

SECURITY CLASSIFICATION OF THIS PAGE (When Data Entered)


FILMED
4-8